POLITECNICO DI TORINO

Dipartimento di Ingegneria Meccanica ed Aerospaziale (DIMEAS)

Tesi di Laurea Magistrale

Breadboarding of optical attitude sensor for space application

Relatore:

Prof. Angelo Lerro

Tutor aziendale:

Dott. Marco Pisani

Candidato:

Claudio Bramante

Acknowledgments

I would like to thank my family who always helped me when I needed it and always pushed me to do more. You have supported me throughout all these years and have always been close to me. Without your efforts I would not be the person I am and I would not have achieved this goal.

Furthermore, I would like to thank my supervisor, Professor Lerro Angelo, for giving me the opportunity to carry out this work and my tutor at INRiM, Pisani Marco, for his valuable guidance during my studies for the completion of the thesis.

Contents

List of Figures

Abstract

The aerospace industry is currently trying to improve the performance of telecommunications satellites and one of the ways to do this is to increase the size of the reflectors, which are expected to be up to 5m in diameter. This increase, however, involves the use of large structures to connect the antenna to the main body of the satellite and, since the rods undergo deformations due to temperature gradients in space, a metrological system is required to know the attitude of the reflector.

In this sense, INRiM (Istituto Nazionale di Ricerca Metrologica - National Institute of Metrological Research) proposes the use of optical metrology based on the exchange of information between the spacecraft and the antenna through light beams. This methodology makes it possible to obtain information through non-contact measurements using small and highly accurate instruments. The instrument designed by INRiM is called ATOM (ATtitude Optical Monitor) and is composed of an Active Unit (AU), which represents the reference system (in this case the main body of the satellite), and a Passive Unit (PU) attached to the target to be monitored (i.e. the reflector). The main purpose of ATOM is to relate the reference system of the antenna to the reference system of the satellite such that it is possible to know the yaw, pitch and roll angles assumed by the reflector.

The purpose of this study is to create an ATOM prototype and to evaluate its effectiveness in terms of maximum detectable angles. For simplicity's sake, two different models were created, the first for evaluating yaw and pitch angles and the

second for evaluating roll angle. The tests carried out show that it was possible to detect a maximum angular variation in pitch and yaw of the target equal to $\pm 0.116°$, while there is no limitation on the roll angle, thus meeting the expectations set by INRiM and requested by ESA.

1. Preliminary study

In the following chapter, the process that led to the realisation of an initial prototype using some of the main elements of the ATOM unit design will be explained in order to familiarise oneself with them. In addition, a Matlab code was implemented that was capable of detecting the position of the spot by analysing the images acquired via a camera and recreating the Gaussian pattern in three dimensions.

1.1   Laser mounting and collimation

To realise the prototype, a breadboard (i.e. an optical plate made of metal material on which holes were drilled at regular distances) was used, on which two supports were mounted: the first to house the laser source and the second for the lens. In addition, to facilitate the collimation process of the laser, an iris was also positioned beyond the lens. These three elements were positioned on the same line and the heights adjusted so that the centres of each element lay on the same optical axis.

The two aforementioned mounts are manufactured by Thorlabs and are respectively a KM100[1] and a KM200[2]: the former has an internal diameter of 25 mm while the latter is 50 mm and both mounts have two rings to be able to adjust the pitch and yaw angles of the housed element.

---

[1]Complete specifications of the mount for the laser source can be found at [5]
[2]Complete specifications of the mount for the lens can be found at [6]
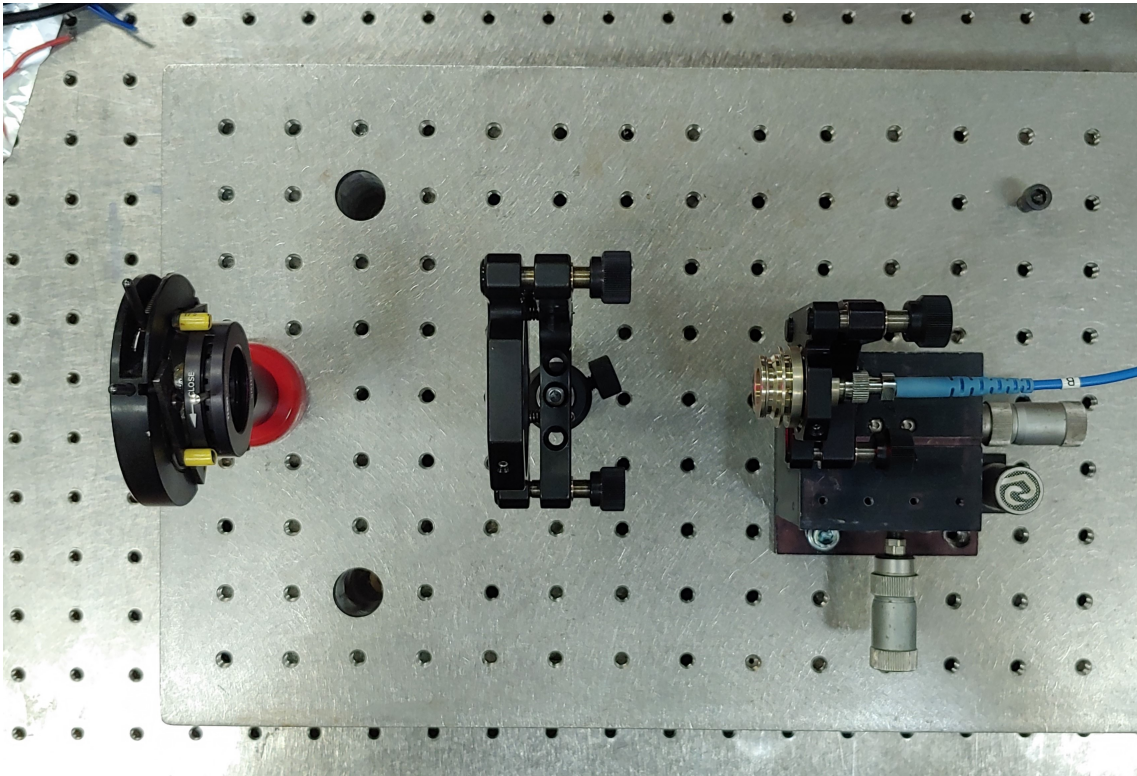
Figure 1.1: Initial setup to perform laser collimation - top view
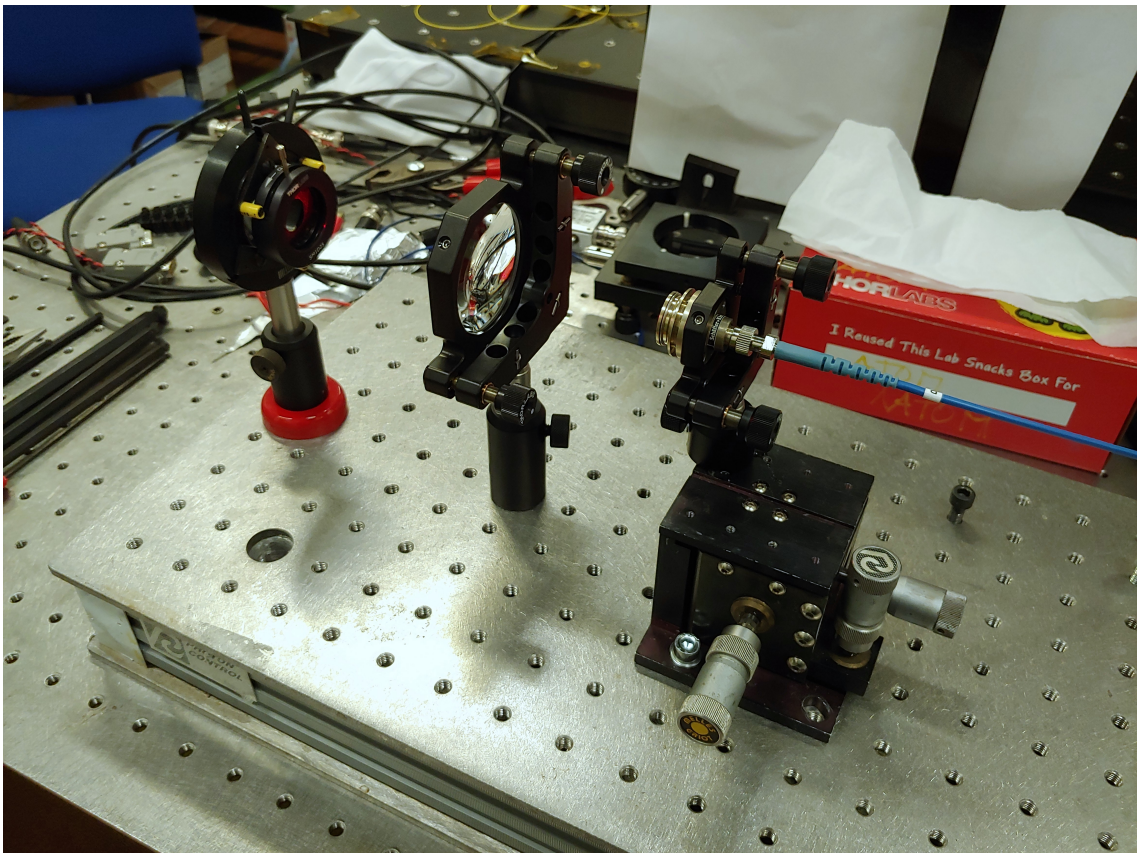
Figure 1.2: Initial setup to perform laser collimation - side view

The laser source used is from a pointer operating in the red spectrum with a wavelength of 633 nm to which an FC/PC fiber optic cable produced by Thorlabs was connected (FiberCable/PhyscicalContact, which allows for direct contact between the surfaces of two connected fibers)[3] so that it can be inserted into the special fiber holder produced by Schäfter+Kirchhoff[4].

The lens used is the same as the lens in the ATOM project proposed by INRiM except for the surface coating, which is not present in this preliminary study and in the rest of the thesis work: it is an aspherical lens with a diameter of 50 mm and a focal length of 100 mm produced by Thorlabs[5]. The peculiarity of this type of lens lies in the fact that the surface has a profile that is neither a portion of a sphere nor a cylinder with a circular base, but typically the surface profile can be traced back to hyperbolas or ellipses. This specific characteristic allows for a more precise light distribution, a lower lens thickness and a reduction in optical aberrations typical of spherical lenses.

As can be seen in Figure 1.1 and Figure 1.2, the laser source holder was mounted on a platform adjustable on three axes thanks to the rotation of the appropriate rings: this allowed the light source to be moved along the longitudinal axis, defined by the optical axis of the lens, so as to position it at a distance from the lens that was equal to the latter's focal length. The configuration described makes it possible to obtain a light beam exiting the lens of a collimated type, characterised therefore by parallel rays and a planar wave front. Visually, this condition can be recognised by the fact that the diameter of the light beam beyond the lens remains constant regardless of the distance at which it is measured.

To check the collimation of the light beam, the breadboard was then placed in a corridor where it was possible to move the target, consisting of a simple square of cardboard with a sheet of graph paper attached to it on which to measure the diameter of the light beam, at a distance of at least 24 m. Starting from the

---

[3]Complete specifications of the fiber optic cable can be found at [9]
[4]Complete specifications of the fiber holder can be found at [1]
[5]Complete specifications of the aspherical lens characteristics can be found at [2]

configuration in Figure 1.3, two sets of images were acquired:

- the first set of photos features the use of the previously mentioned iris set at an aperture of 3/4 of the total, which allows for a bright circle with well-defined edges;

- the second series of photos presents images taken without the use of the iris, resulting no lobger in a beam with defined edges but in a luminous circle with a Gaussian pattern.

In both cases, six images were acquired by positioning the target at different distances: 1 m, 2 m, 4 m, 8 m, 16 m and 24 m.

Figure 1.3: Verification of light beam collimation

Images acquired both with and without the iris are shown next:

(a) Target at 1 m   (b) Target at 2 m   (c) Target at 4 m

(d) Target at 8 m   (e) Target at 16 m   (f) Target at 24 m
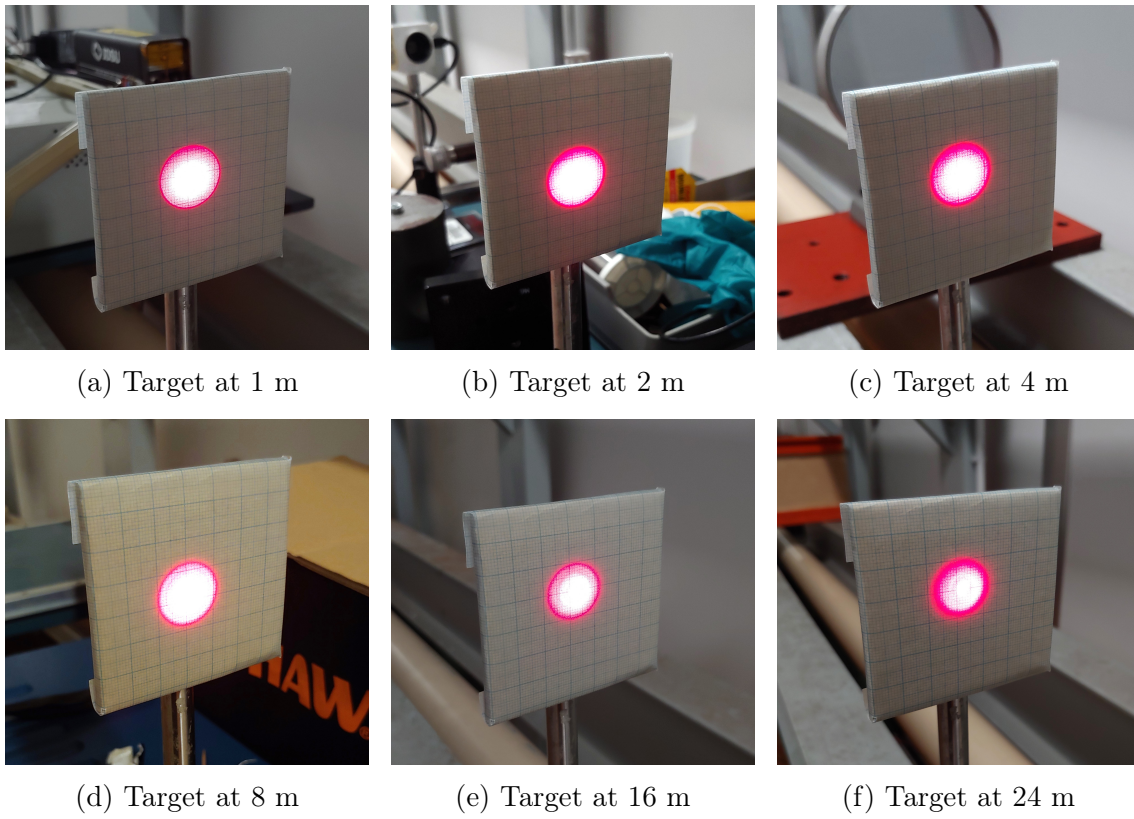
Figure 1.4: Light beam diameter at different distances with the iris

(a) Target at 1 m   (b) Target at 2 m   (c) Target at 4 m

(d) Target at 8 m   (e) Target at 16 m   (f) Target at 24 m
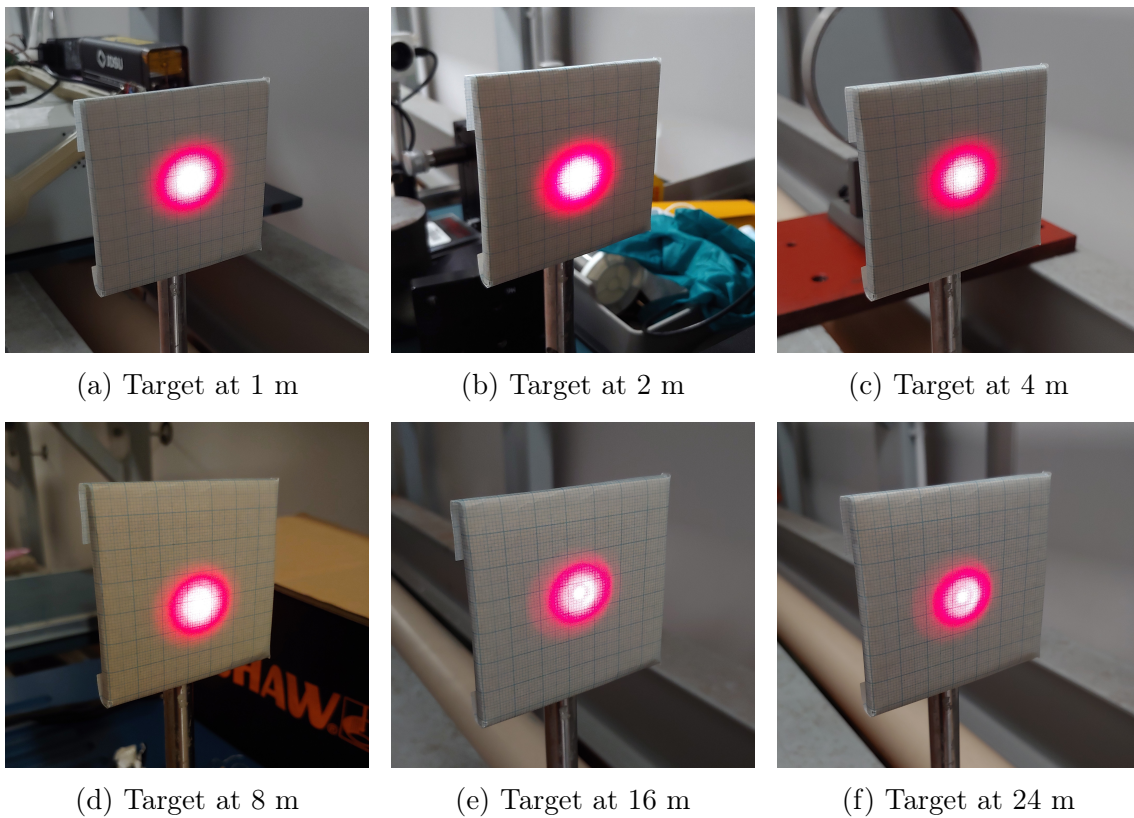
Figure 1.5: Light beam diameter at different distances without the iris

As can be seen in Figure 1.4, the diameter of the light beam is about 23 mm, net of slight diffraction phenomena that are visible especially when the distance is increased. Analysing the second set of images in Figure 1.5 without the use of the iris, it is possible to state that the light beam is rather collimated since it has a diameter of approximately 37 mm at any distance. Furthermore, there is a slight lateral shift of the light beam and this generates an image on the target that is asymmetrical as can be seen in Figure 1.5f: since the ATOM design involves the positioning of the PU at no more than 8 m, this phenomenon, which is mainly present at 24 m, is neglected.

Finally, after establishing that the set distance between the laser source and the lens was the optimum to obtain a collimated light beam, the red laser was replaced with an infrared laser operating at a wavelength of 830 nm, similar to one of the two lasers in the ATOM project.

1.2 Image acquisition and processing

After collimating the laser beam, three more elements were added to the breadboard: a mirror, a beam splitter and an image sensor.

The mirror was mounted on a stand identical to that of the lens, namely a KM200 from Thorlabs, and was positioned so that it was at the same height as the lens.

A beam splitter[6] is an optical device that divides an incident beam of light into two parts, one transmitted and the other reflected. There are different types of beam splitters and in this case a flat beam splitter was used, i.e. a glass layer with a thin, partially transparent metal coating whose thickness is defined so as to have a specific ratio between transmitted and reflected light. The beam splitter was of course also positioned so that it was at the same height as the other elements, but using a fixed support because precise angular adjustment was not necessary as long as it was at approximately 45°.

---

[6]Complete specifications of the beamsplitter can be found at [3]
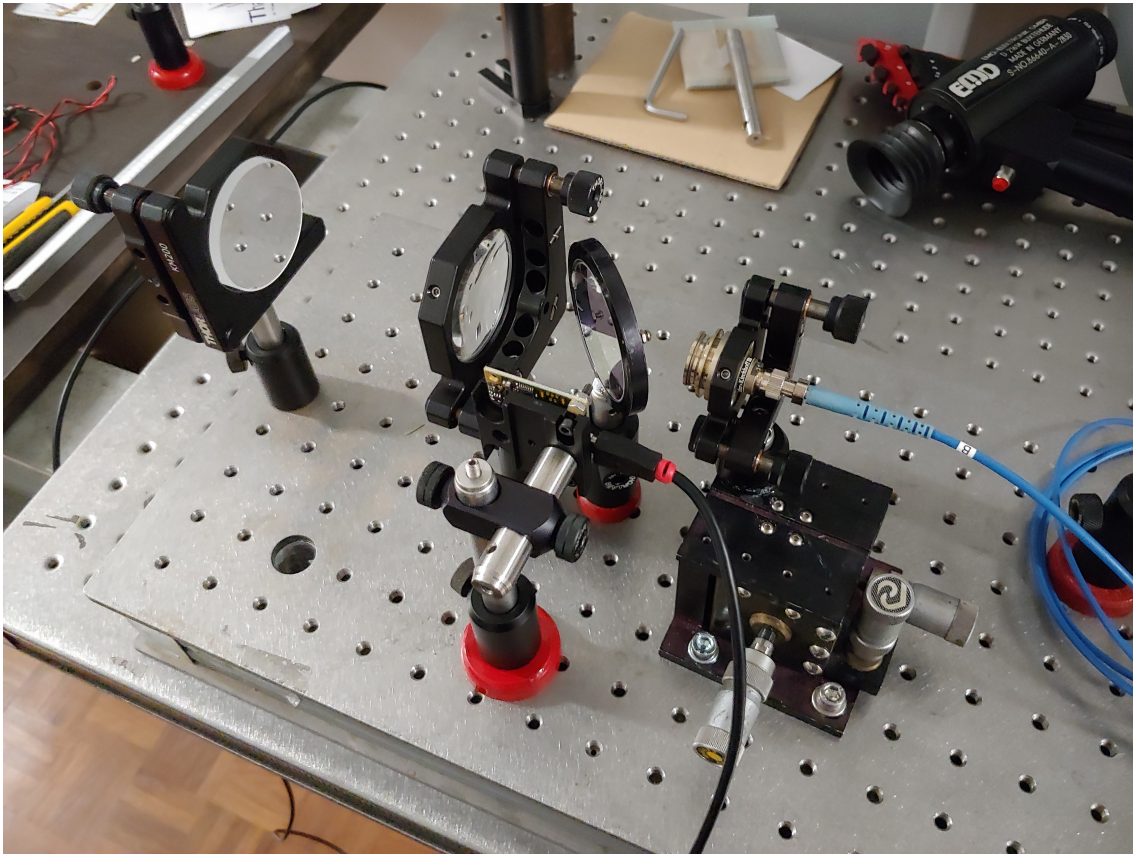
Figure 1.6: Modified setup to acquire images

Finally, the sensor was positioned in front of the beam splitter in order to receive the light beam along the path back to the centre of the useful area in an orthogonal manner. In addition, the distance between the beam splitter and the sensor was adjusted so as to detect a perfectly focused light spot on the sensor, in fact in Figure 1.6 it is possible to observe that the distance between the source and the lens and the distance between the lens and the sensor is the same. This made it possible to acquire images showing a light spot with a diameter of about 10 pixels: the sensor used has a pixel size of 5.2 μm, which translates into a light spot diameter of about 50 μm.

As mentioned earlier, the KM200 support is equipped with two rings that allow the pitch and yaw angles of the hosted element to be varied: specifically, each complete turn corresponds to a variation of 0.3°. Knowing this, several images were acquired by varying the yaw angle of the mirror, thus simulating an angular variation of the reflector mounted on the satellite. Starting from the condition in which the

laser beam intercepted the sensor in the centre of the latter, seven images were acquired, from -0.9° to +0.9°, with a step of 0.3° (for simplicity, only the yaw angle variation will be presented, but a similar reasoning also applies to the pitch angle).

The software used for image acquisition is uEye Cockpit from IDS Imaging, a company that produces industrial cameras. In order to obtain useful images for the subsequent analysis, the following precautions were adopted: the exposure time was set to the minimum value, so as not to over-saturate the image in the presence of the light spot with the risk of losing too much information, and all automatisms in terms of image gain and exposure were deactivated.

Below is an example crop of the image acquired with the angle between the mirror axis and the lens axis equal to 0°:
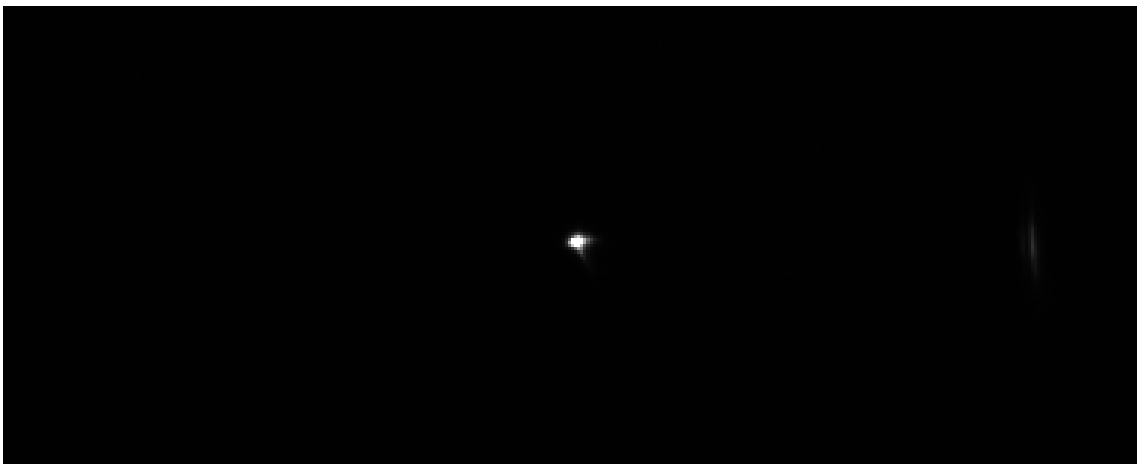
Figure 1.7: Bright spot with 0° mirror angle

As can be seen in Figure 1.7 on the right side of the image it is possible to notice another area of the sensor illuminated by the laser beam: this is most likely due to the presence of the beam splitter because the light beam affects the two surfaces of the optical element at two different distances and this generates astigmatism phenomena.

After acquisition, the images were imported into the Matlab environment in the form of value matrices where they were refined so as to avoid considering spurious signals such as the one just described. Firstly, the pixel at which the maximum intensity was present was identified and used as the centre of a square having a

size of 40x40 pixels so as to zero all points outside the latter (similarly, a threshold could also be set in terms of intensity below which to zero the pixel value but this would not eliminate spurious signals in the event that they had a value above the threshold): by doing so, there is no risk of invalidating the image as the spot has a diameter of just 10 pixels and definitely falls within this much larger square. Secondly, after obtaining 'clean' images presenting only the light spot of our interest, the matrix centroid was calculated for each image using the operators within the Matlab software, thus being able to identify with good approximation the centre of the light spot incident on the sensor.

This made it possible to correlate the angle set on the mirror with the horizontal position of the light spot measured in pixels and derive a trend thanks to which it is possible to know the angular variation starting from the position of the spot. The trend just described is shown below:
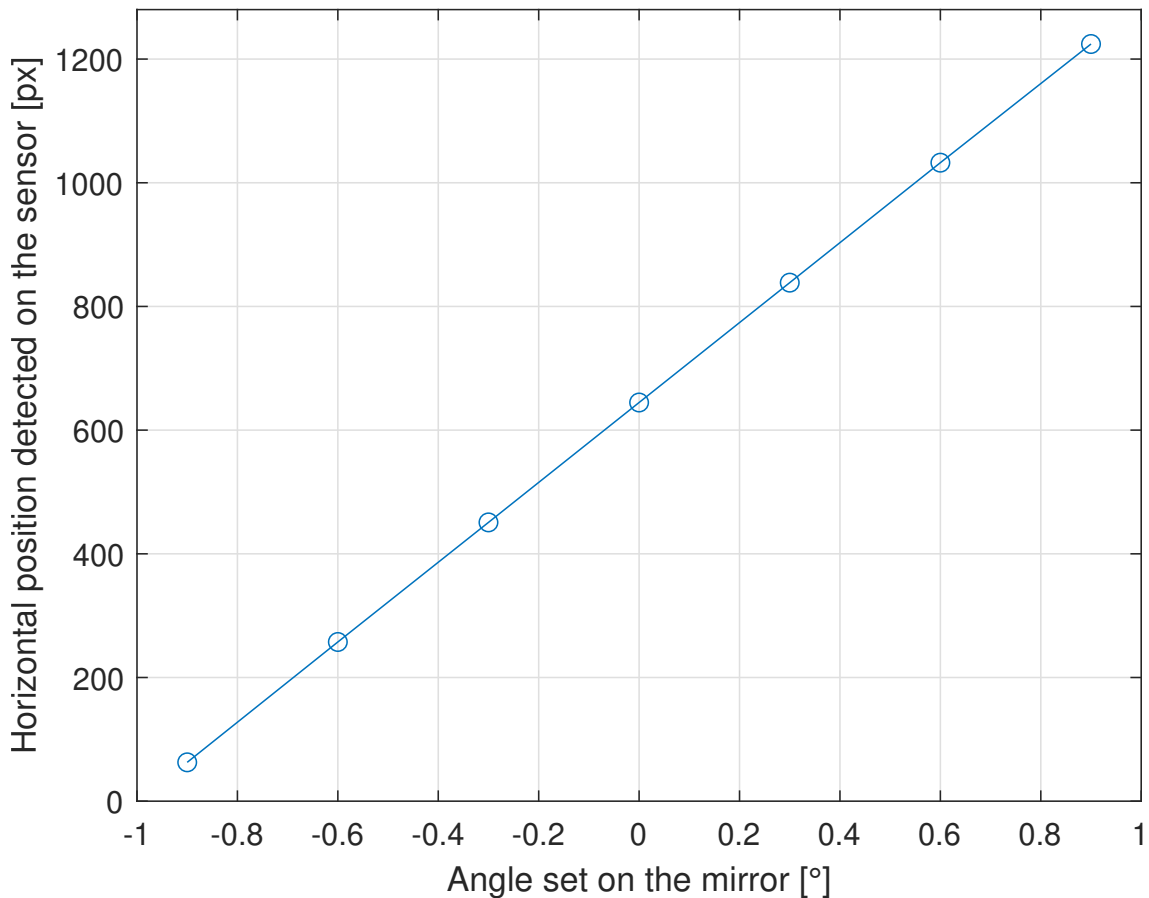
Figure 1.8: Relationship between the angle set on the mirror and the horizontal position detected on the sensor

After doing so, thanks to appropriate geometric relations and exploiting the approximation that for small angles the tangent of an angle is equal to the angle itself, it was possible to express the distance between the positions assumed by the light spot in angular terms and obtain the relationship between the angle set on the mirror and the angle detected analytically through the images acquired by the sensor:
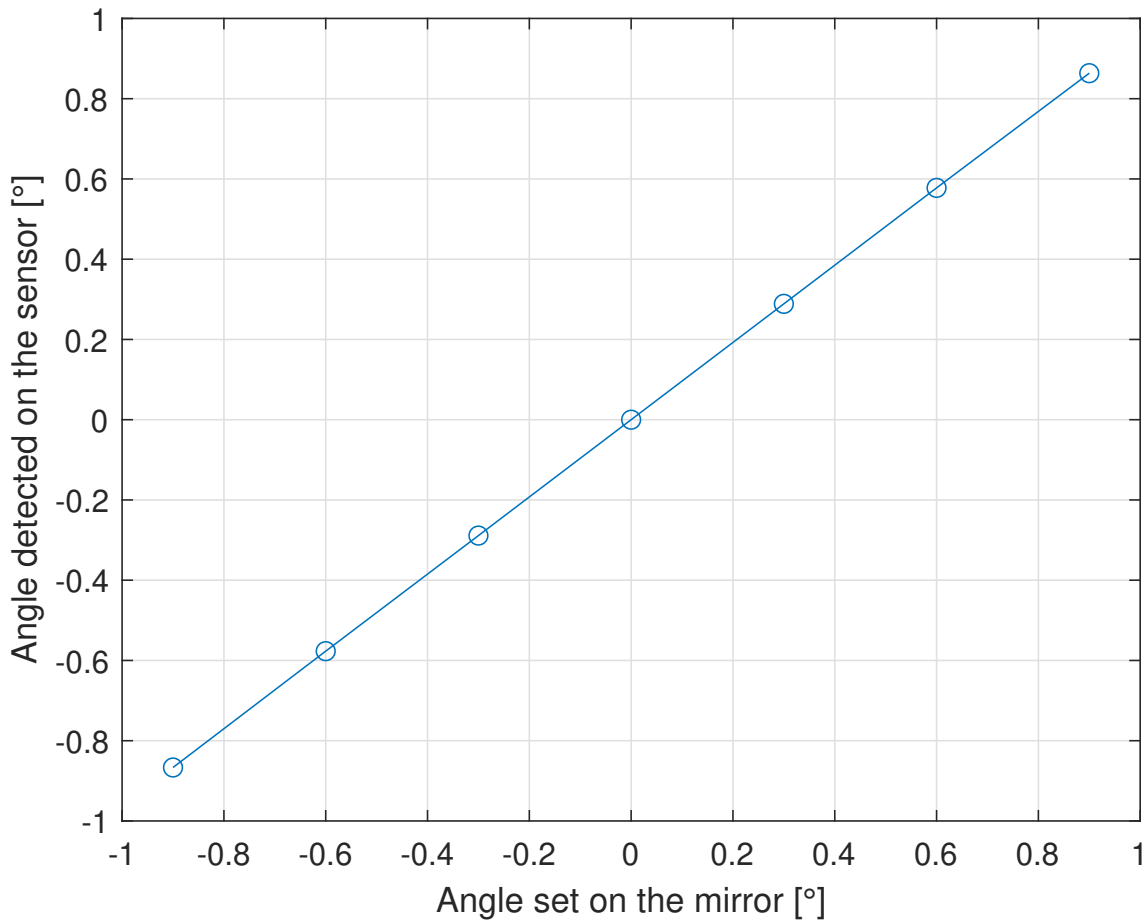
Figure 1.9: Relationship between the yaw angle set on the mirror and the yaw angle detected by the sensor

As can be seen in Figure 1.9, the calculations carried out deviate little from the actual situation, and the relationship presents a linear trend: this means that by knowing how many pixels the light spot on the sensor has shifted, it is possible to know the change in the yaw angle of the mirror to a good approximation. In the following chapter, this study will be expanded upon to estimate the error committed.

Finally, thanks to the use of another Matlab code, it was possible to reconstruct the three-dimensional Gaussian bell of the acquired light spot by making a fit using special functions and calculating its maximum intensity, its effective centre, the angle defining the main axes of the Gaussian expressed in radians and the standard deviations on these axes. For simplicity's sake, the complete images were not analysed, but only portions with dimensions of 100x100 pixels. Below is the fit of the image acquired with the angle between the mirror axis and the lens axis equal to 0°:
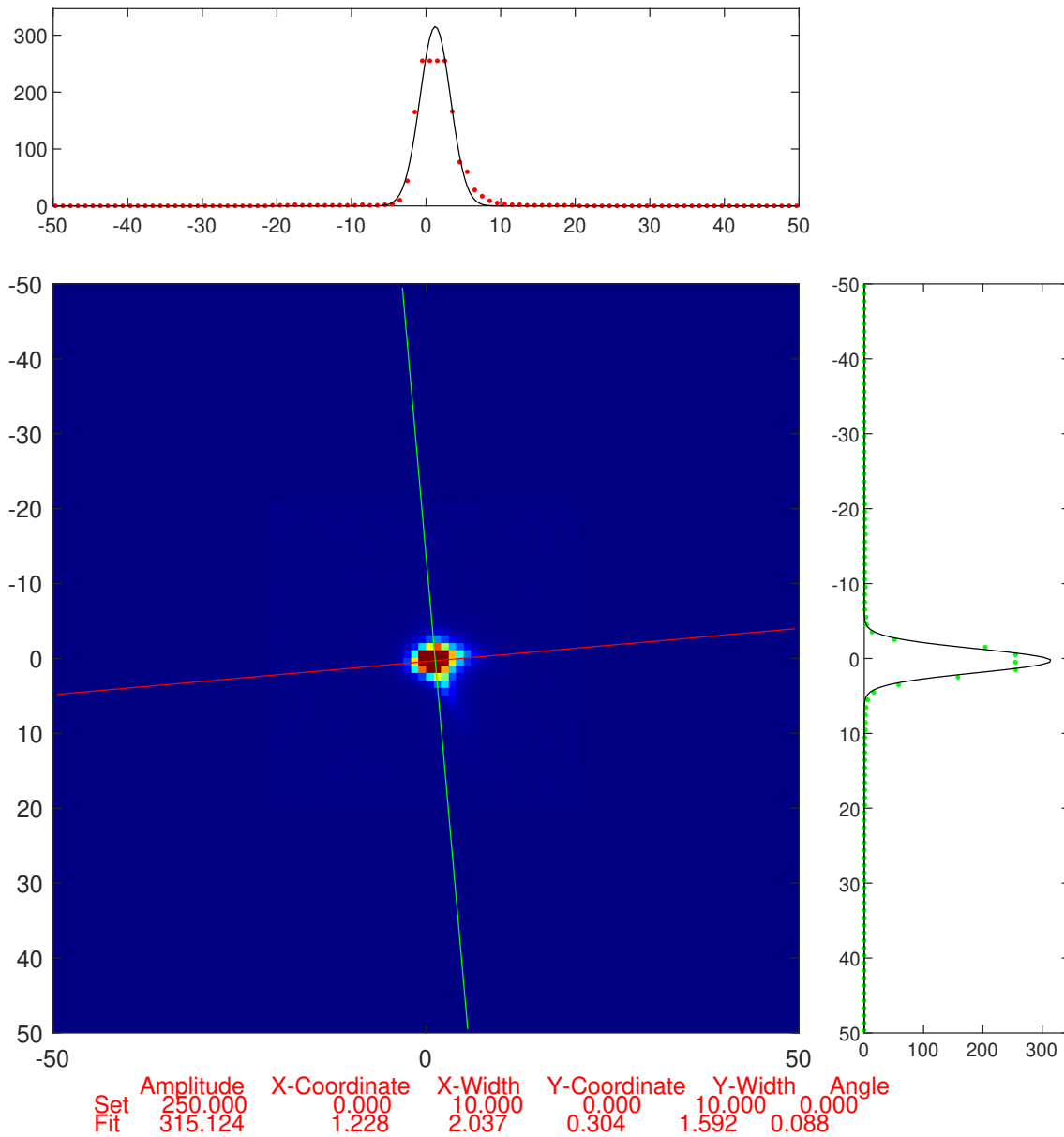
Figure 1.10: Gaussian fit of the light spot - Top view
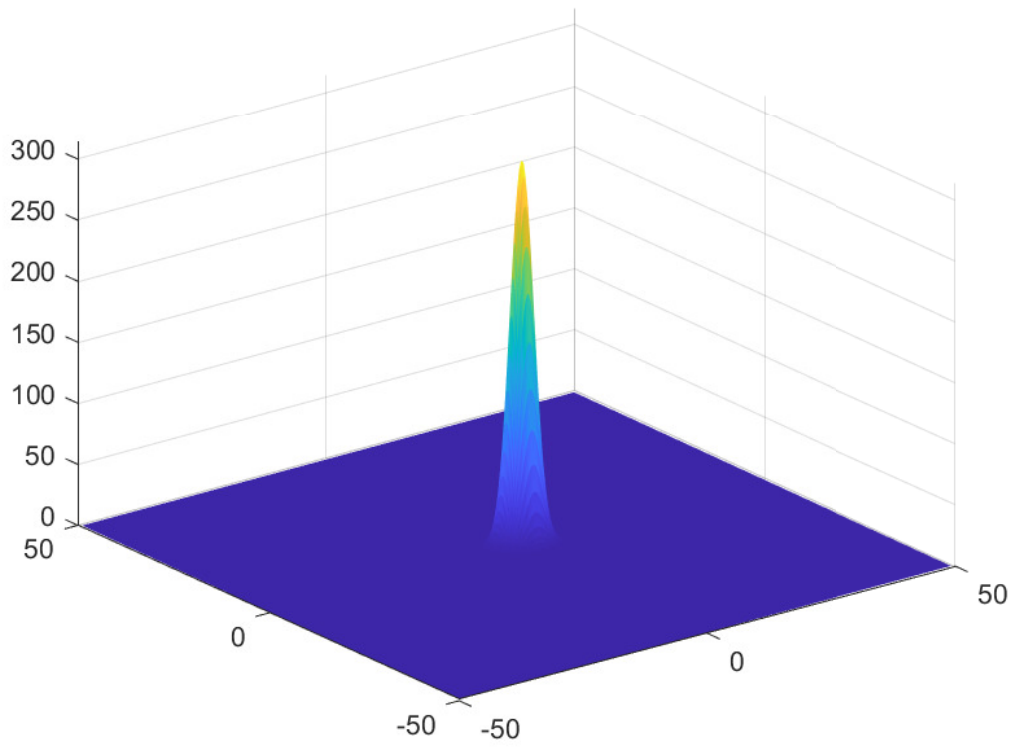
Figure 1.11: Gaussian fit of the light spot - three-dimensional view

2. New AU configuration

In the following chapter, a more in-depth study of the relationship between the angle applied by the mirror and the angle detected by the sensor with the addition of new elements and a different arrangement will be presented.

2.1   Elements added to the setup

On the breadboard used previously, a second beam splitter was added and the sensor was replaced with the one from the ATOM project. In addition, the light source was moved close to the lens and the arrangement of the optical elements and the sensor was modified in order to obtain a configuration of the AU as close as possible to the design realised by INRiM.

As can be seen in Figure 2.1, the design realised by INRiM involves the use of two laser sources operating at different wavelengths, specifically 850 nm and 905 nm, in order to obtain two measurements simultaneously and thus relate the attitude of two different points on the satellite: with this configuration, it is necessary to use a dichroic mirror to separate the two beams in orthogonal directions but, in order to simplify the practical realisation of the system, it was decided to use a single laser source (i.e. the previously used infrared source operating at 830 nm) and neglect the use of this element.
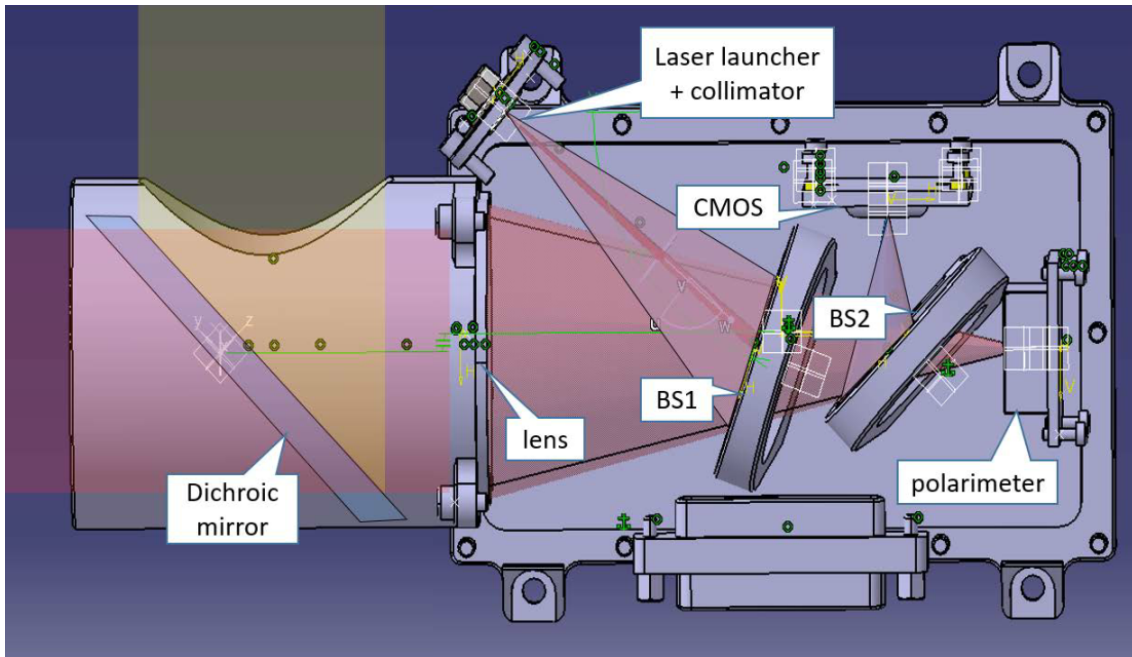
Figure 2.1: Active Unit design created by INRiM

The following is the AU configuration realised in the laboratory so that it was as close as possible to the one envisaged by the ATOM project:
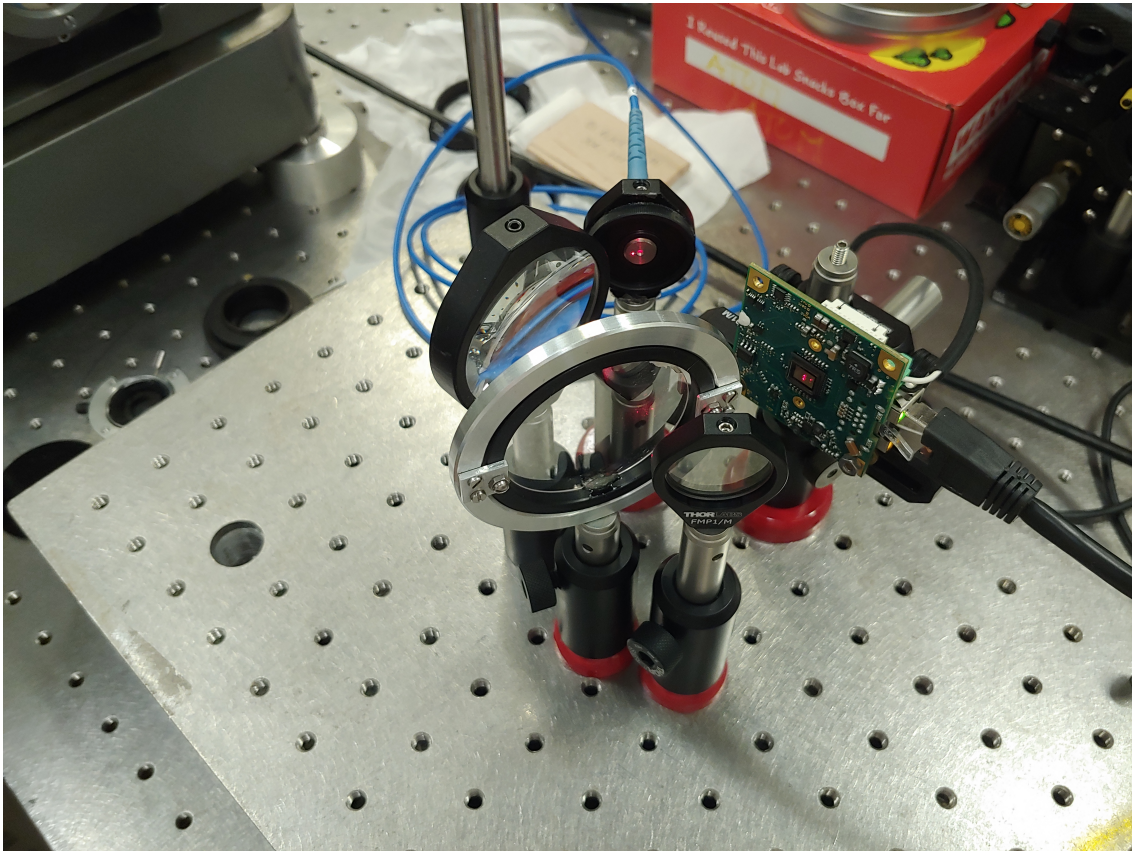
Figure 2.2: AU configuration similar to that envisaged by the ATOM project

The configuration shown in Figure 2.2 also differs in the absence of the polarimeter positioned after the second beam splitter, provided by the design to measure the roll angle: this specific element will be dealt with later in a separate chapter.

The sensor used is the Onsemi MT9P031 CMOS: this type of sensor has been adopted for years in digital photography and smartphones. It has a width of 2592 pixels and a height of 1944 pixels with an overall resolution of 5 MegaPixels, and the single pixel size is 2.2 μm both vertically and horizontally[7].

In this configuration, the larger beam splitter was positioned so that the angle between its reference axis and the optical axis of the lens was approximately 25°, while the second beam splitter, positioned behind the first, has an angle of approximately 45° so that it reflects the laser beam orthogonally to the sensor.

Finally, in order to make more precise angular variations than in the previous case, the mirror was replaced with another instrument which allows variations to be made with greater precision. The instrument used is shown below:
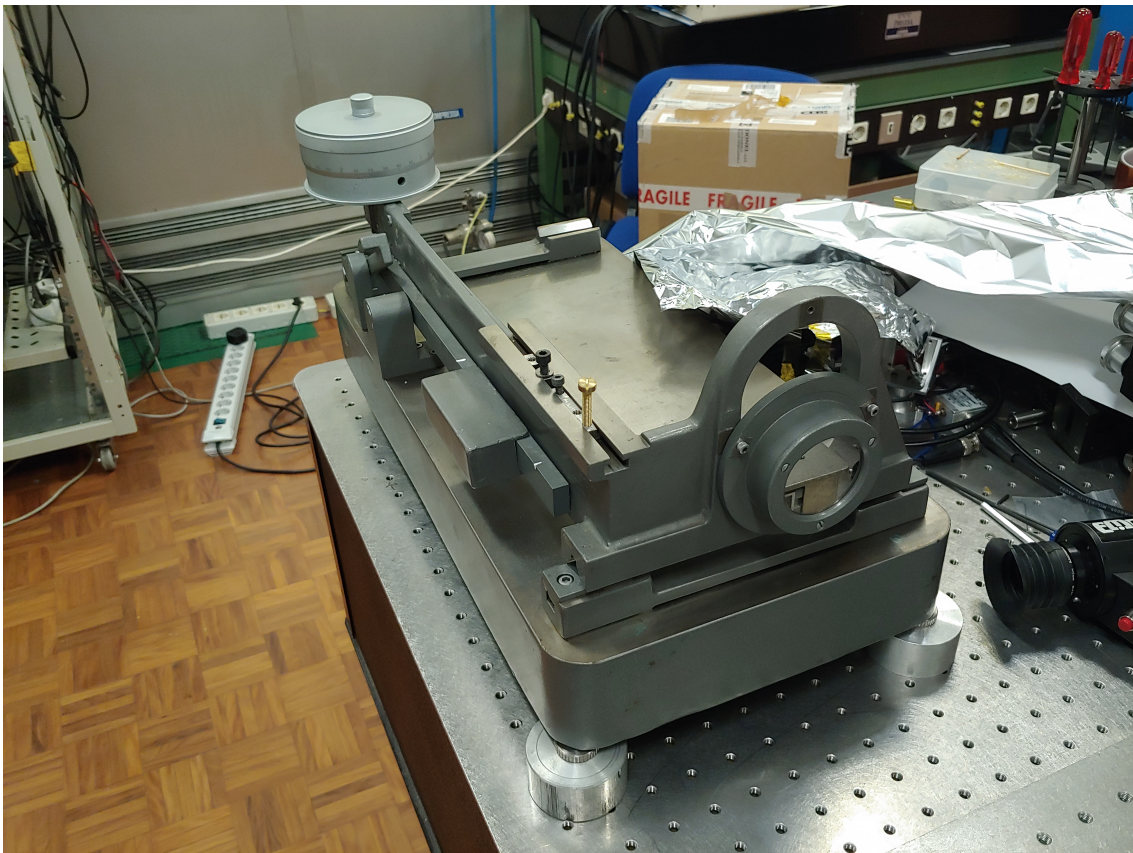
Figure 2.3: Tool used to vary the pitch angle of the mirror

---

[7]Complete specifications of the sensor can be found at [8]

As can be seen in Figure 2.3, a mirror with the same dimensions as the previous one has been mounted on the front part of the instrument, while on the rear part there is a graduated ring nut that allows, through its rotation, to vary the pitch angle of the mirror. The scale on the ring nut is expressed in arcseconds and the resolution of the instrument is equal to the tenth of an arcsecond: knowing that one arcsecond is equal to $1/3600°$, we obtain an equivalent resolution of $2.\overline{7}$e-5°.

2.2 Calculation of the error between applied angle and detected angle

Similarly to what was done previously, several images were acquired by varying the mirror's pitch angle: in this case, always starting from the condition in which the laser beam intercepted the sensor in the centre of the latter, nine images were acquired with a size of 400x400 pixels, from -360 arcsec to +360 arcsec, with a step equal to 90 arcsec, i.e. from -0.1° to +0.1° with a step equal to 0.025°.

After the images had been acquired, they were imported into the Matlab environment in the form of value matrices and 'cleaned' for subsequent analysis by following the same procedure as before: the pixel containing the maximum intensity was identified and all remaining pixels located at a certain distance from it were set to zero.

After doing so, as in the previous chapter, through geometric relations and analytical calculations, the distance between the positions of the spots was derived in angular terms, so that a relationship could be expressed between the angle set on the mirror and the angle detected by the sensor.

The two graphs obtained are shown below: the first represents the relationship between the angle set on the mirror and the vertical position detected by the sensor, while the second represents the relationship between the angle set on the mirror and the angle detected by the sensor:
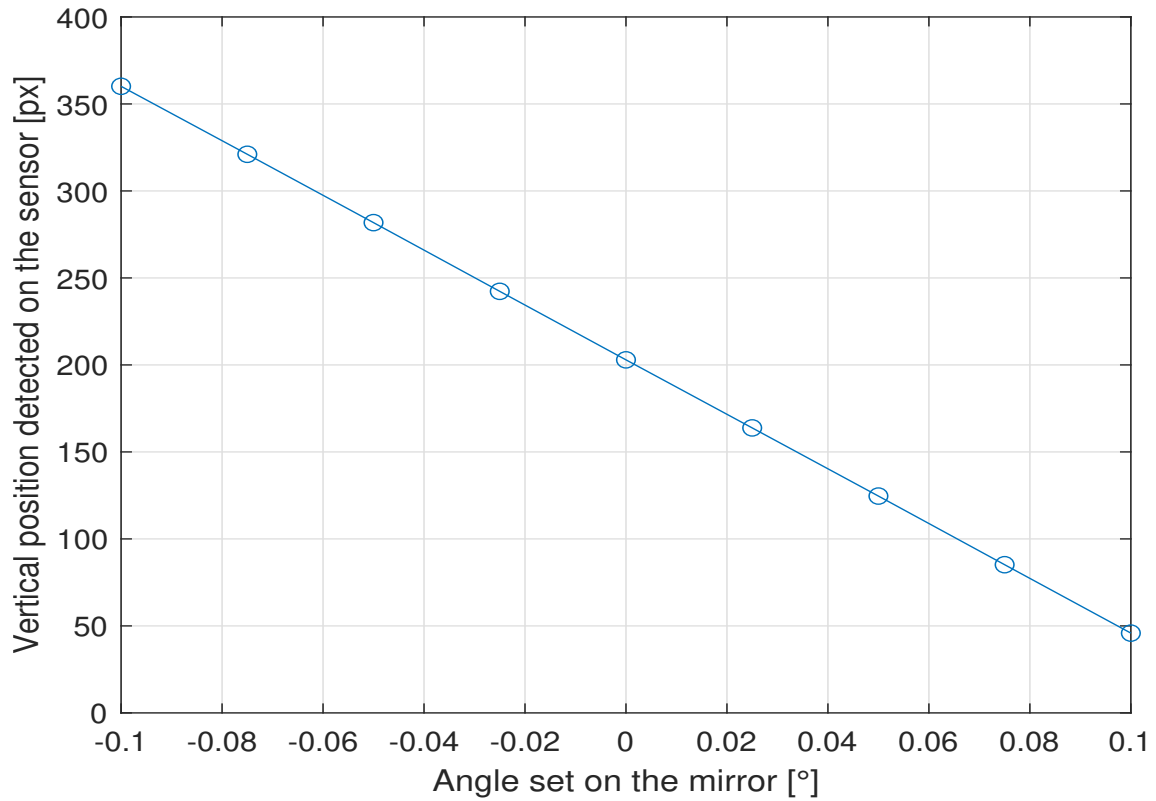
Figure 2.4: Relationship between the angle set on the mirror and the vertical position detected on the sensor
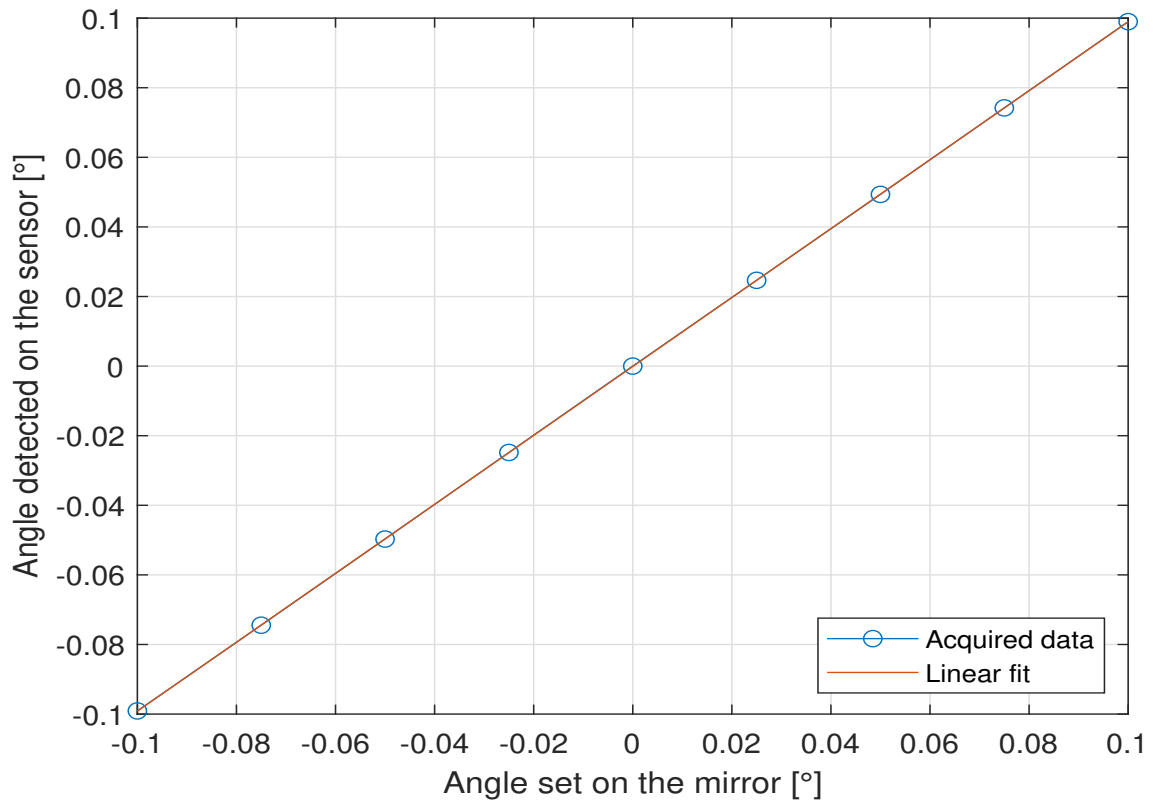
Figure 2.5: Relationship between the pitch angle set on the mirror and the pitch angle detected by the sensor

Finally, as can be seen in 2.5, the relative fit of the acquired data was also calculated in order to recreate an exactly linear trend between the applied angle and the detected angle: thanks to this, it was possible to determine the relative residuals at each point between the two functions in the graph.
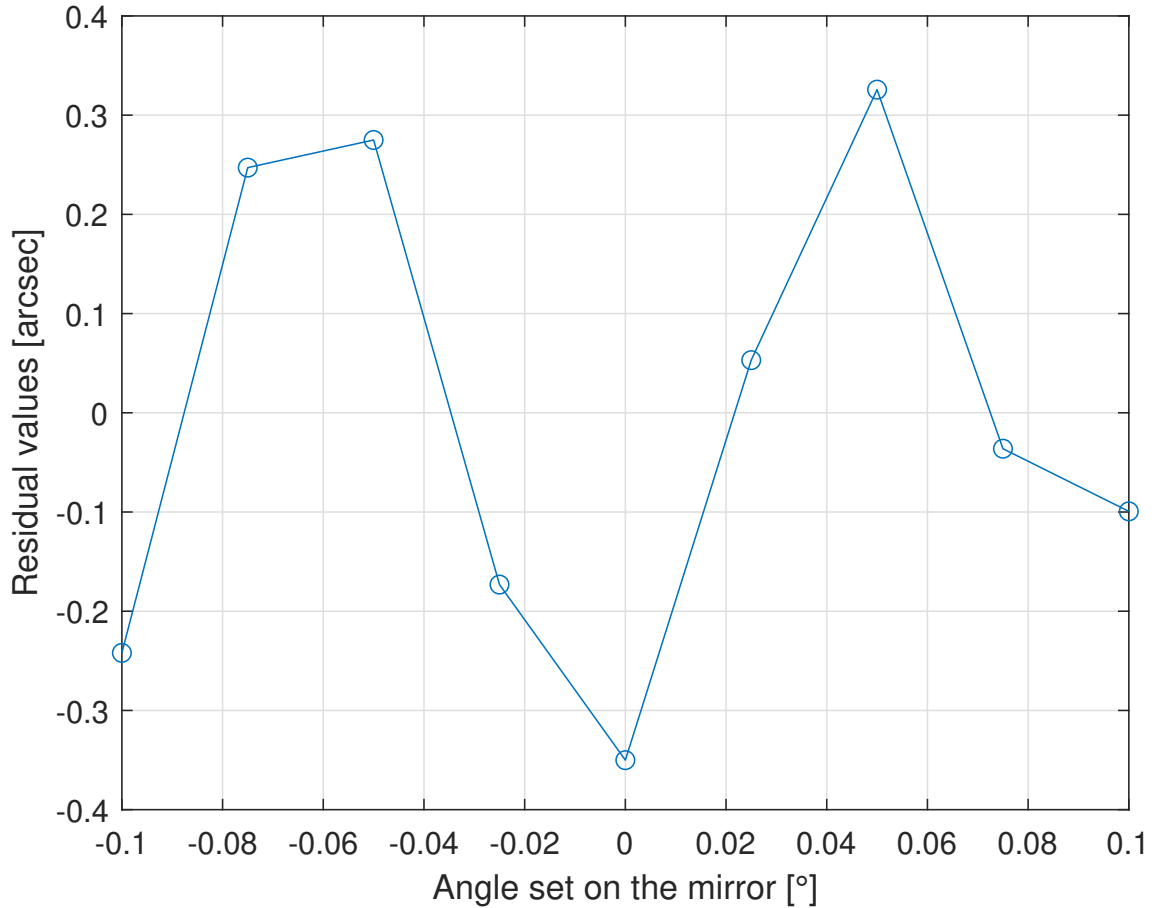
Figure 2.6: Linear regression residuals

Observing Figure 2.6, it can be seen that the largest residual is 0.35 arcsec, or 9.7e-5°: this result leads to the conclusion that the errors committed are 3 orders of magnitude smaller than the magnitudes involved and that the calculations performed provide an acceptable estimate of the mirror's pitch angle.

3. Estimation of the angular variation detectable by the instrument

In the following chapter, the process that led to the realisation of the final configuration of the prototype, i.e. as similar as possible to that envisaged by the ATOM project, both with regard to the AU and the PU and the path between them, will be explained. In addition, calculations were carried out again with regard to the yaw angle variation of the mirror located at the end of the path (since the angular change in yaw is equivalent to that in pitch and vice versa) in order to actually establish how large the maximum angular variation detectable by the instrument was.

3.1 Integration of AU and PU spacing

In the design of ATOM envisaged by INRiM, the PU must be at a maximum of 8 m from the AU, so a path approximately 8 m long was recreated at the end of which the PU was to be positioned, which in this case is represented as usual by a mirror with the possibility of varying the yaw angle and the pitch angle through the use of two special rings. In an attempt to maintain as compact an arrangement as possible on the lab table, several mirrors were used to create the path between the AU and the PU (more precisely, five mirrors mounted on supports to adjust the attitude). The setup achieved can be seen in Figure 3.1:

Figure 3.1: Final prototype configuration
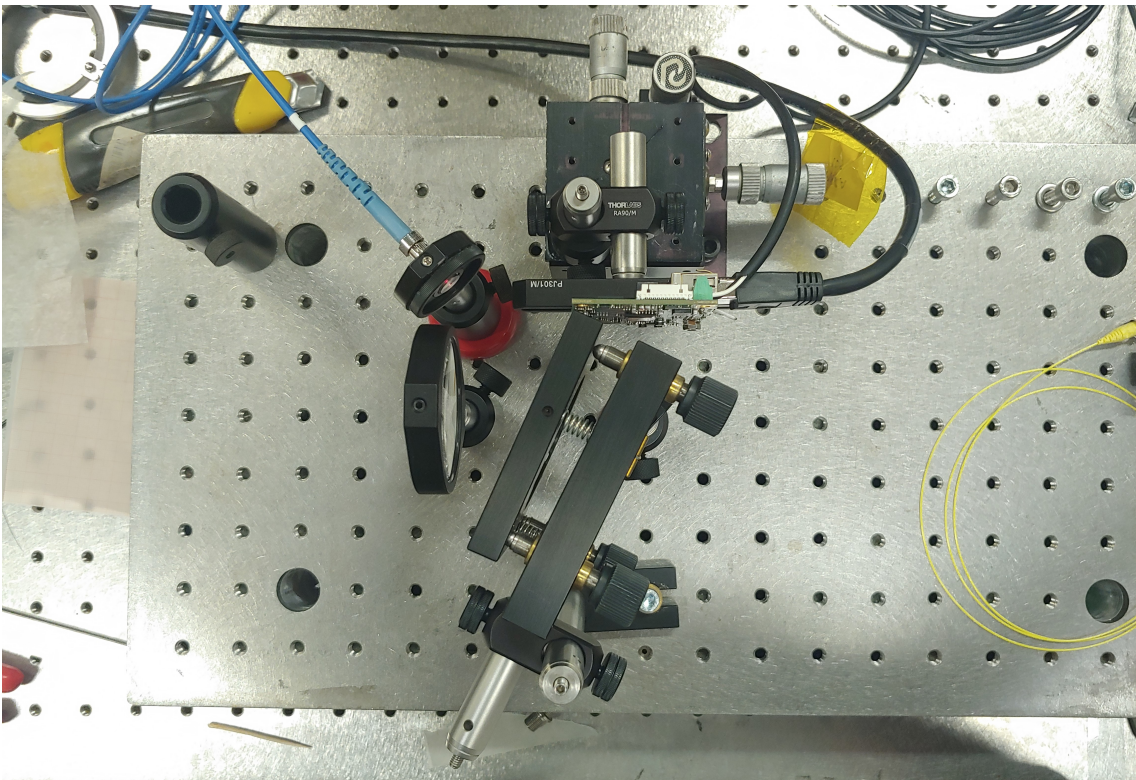
Figure 3.2: Final AU configuration - Top view

After this was done, minor changes were also made to the AU while still retaining the same elements, more specifically the sensor and first beam splitter mounts were changed in order to have more control over the attitude adjustment of the latter: the sensor was mounted on the same three-axis adjustable platform as previously seen, while the first beam splitter was placed inside a bracket similar to those found in the previous chapters, which allow the yaw and pitch angle of the housed element to be varied.
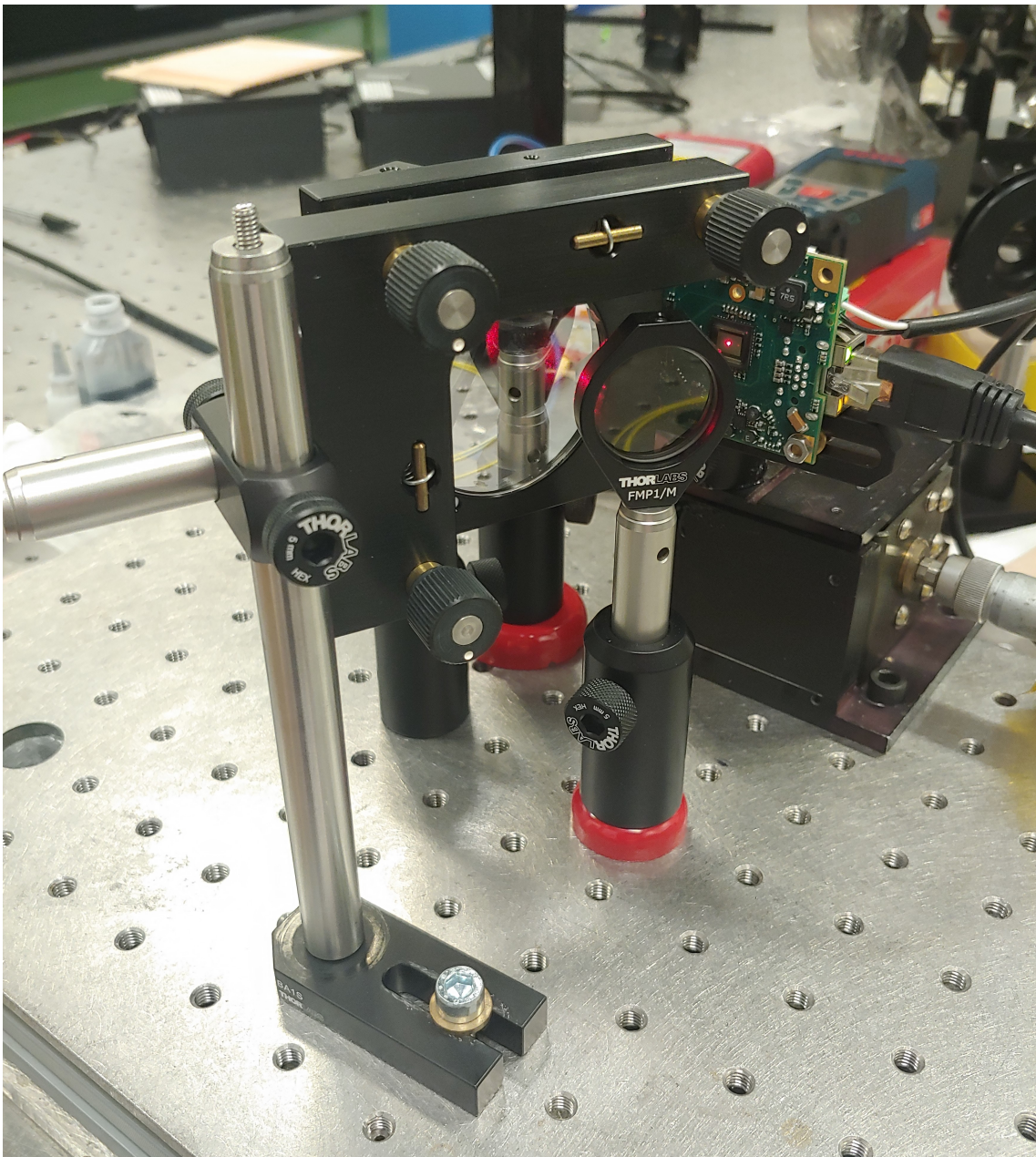
Figure 3.3: Final AU configuration - Side view

3.2 PU calibration

The mirror used as a PU located at the bottom of the path is inserted inside a frame which also includes two ring nuts for adjusting the yaw and pitch angles but, unlike the supports seen previously, the latter has two different scales on each ring nut and furthermore these scales are not easily attributable to angular variations. To find out how much each notch on the graduated scale on the two rings of the mirror corresponds, an autocollimator was used, specifically the ELCOMAT 3000 produced by the company Möller-Wedel Optical[8]. The autocollimator is an instrument that uses internal optics to measure angles and is typically used to align optical instruments. After mounting it in front of the PU it was therefore possible to independently rotate the two rings of the mirror and obtain the corresponding angular variation expressed in arcseconds from the autocollimator display.
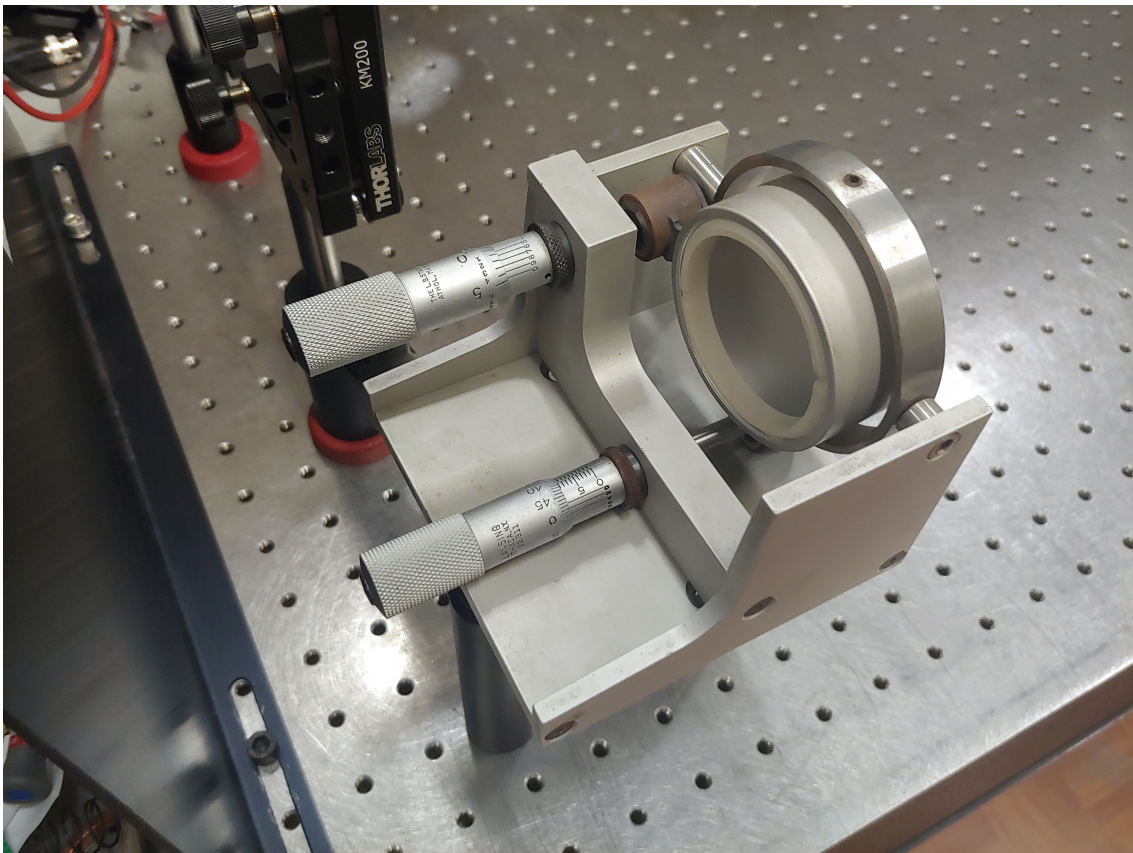
Figure 3.4: Final PU mirror

---

[8]The instrument has been replaced by the recent ELCOMAT 5000, complete specifications of this autocollimator can be found at [4]
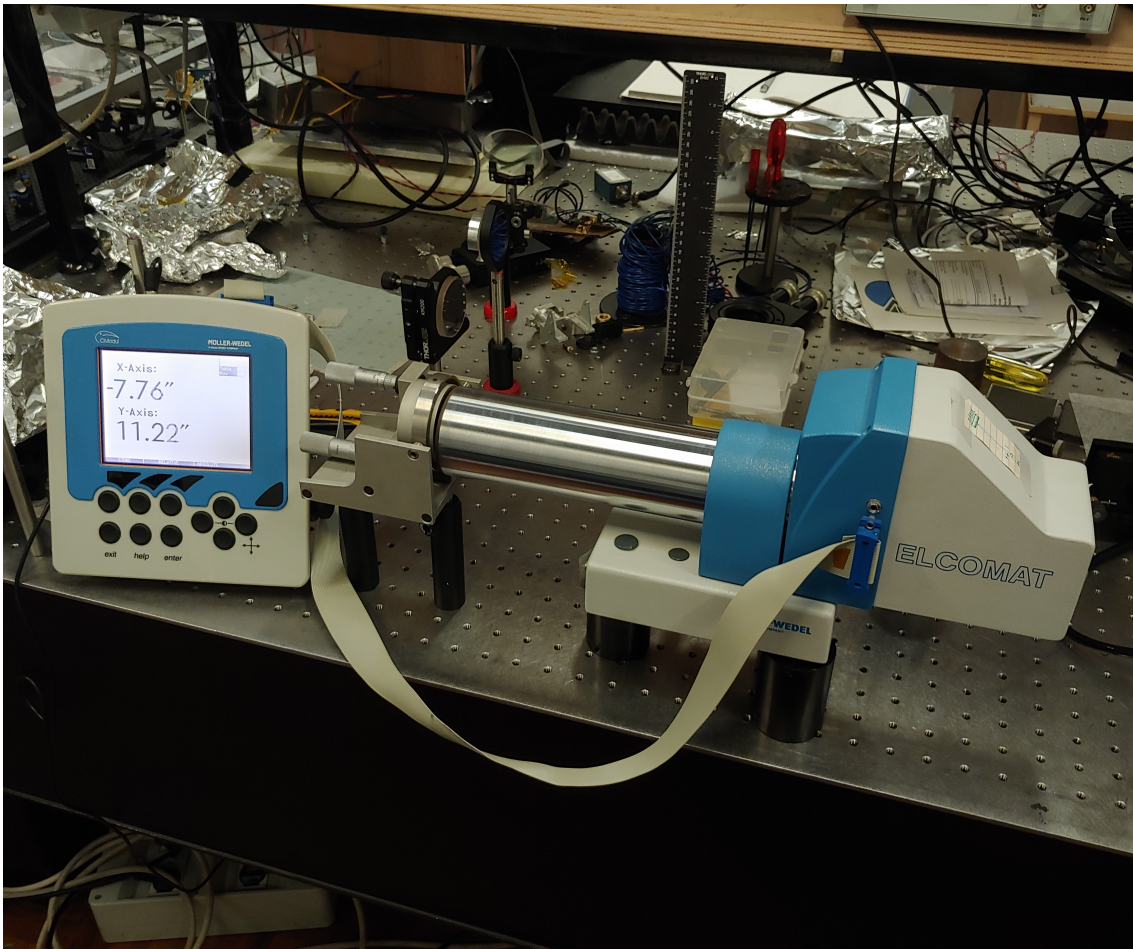
Figure 3.5: Autocollimator

About ten angular variations were then made in terms of both yaw angle and pitch angle and the relative readings given by the collimator were noted down. Finally, by recreating a law relating the variations made to the readings of the instrument, it was possible to derive the angular variation expressed in degrees relative to each notch on the two rings of the PU support relative to the yaw angle and pitch angle: in the first case, there is a resolution of 0.037465° for each notch while in the second case there is 0.014102°.

This will be useful later as it will allow us to determine whether the maximum angular variation calculated in terms of yaw angle and pitch angle corresponds to the rotations applied on the two mirror rings.

3.3   Determination of maximum yaw/pitch angle

After having calibrated the mirror, several images were acquired again by varying the yaw angle of the PU: specifically, the mirror ring was rotated so as to obtain eight images with a size of 400x400 pixels with a distance of the light spot between one image and the next of about 30 pixels.

After capturing the images, they were imported into the Matlab environment and 'cleaned' for subsequent analysis, thus zeroing out pixels located far from the light spot.

Finally, in order to determine how much was the horizontal span covered by the light spot expressed in pixels, the graph representing the relationship between the horizontal position of the spot and the light intensity of the latter was derived by calculating the double integral. The trend just described is shown below:
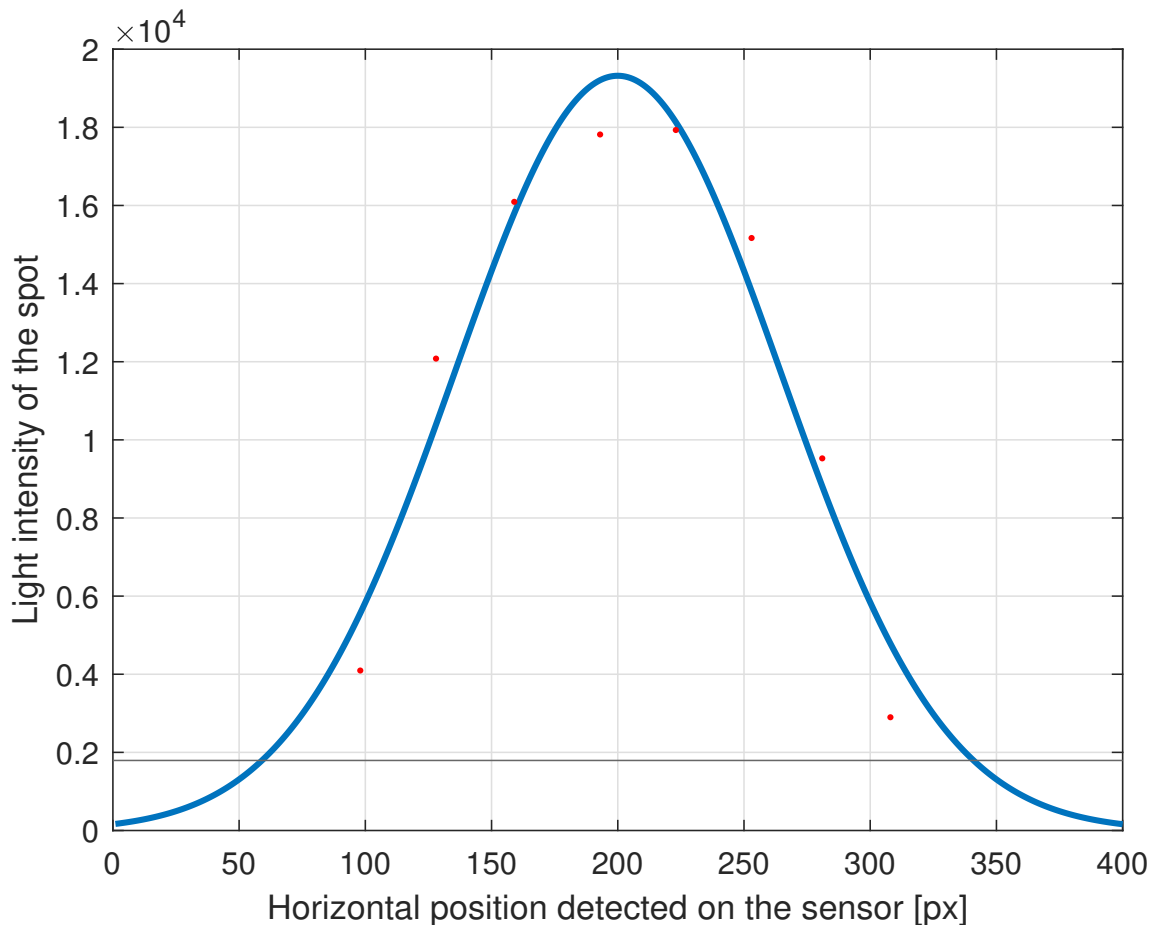
Figure 3.6: Relationship between the horizontal position detected on the sensor and the light intensity when the beam is collimated

As can be seen in Figure 3.6 the function that best interpolates the acquired data turns out to be the Gaussian function. Applying a minimum threshold equal to 10% of the maximum intensity below which spot detection is not considered acceptable, a horizontal span equal to approximately 282 pixels was obtained which, by means of appropriate analytical calculations, corresponds to approximately 0.17945°: this result is in line with the rotation applied on the mirror's ring-nut since from the first to the last image almost five notches were covered, with an angular variation equal to approximately 0.18°.

Furthermore, the result obtained is in agreement with the geometry of the system. Figure 3.7 shows a schematisation of the prototype realised in the laboratory with the PU at a distance of 8 m from the AU: to calculate the maximum angle of the laser beam entering the lens, since these are small angles, it is sufficient to simply make the ratio between the minor cathetus and the major cathetus of the triangle highlighted in the figure, where the minor cathetus represents the radius of the lens and the major cathetus represents the distance between AU and PU. Finally, by transforming the angle obtained from radians to degrees, and remembering that each angle applied to the mirror corresponds to twice the angular variation of the laser beam, we obtain a maximum variation of the PU of approximately 0.179°.
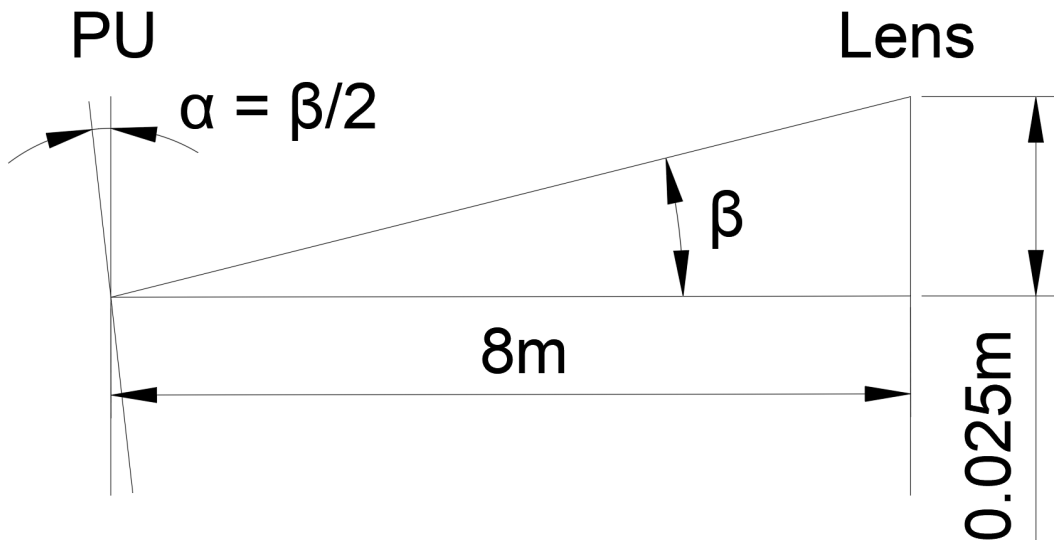
Figure 3.7: Maximum angle detectable by AU

3.4   Laser beam divergence

One of ESA's requirements for INRiM is that the ATOM sensor should be able to detect an angular variation of the light spot of $\pm 0.1°$ from the reference position, i.e. slightly more than if the laser beam were collimated. A possible solution to this problem is to slightly modify the arrangement of the elements so as to reduce the length between the source and the lens, thus obtaining a divergent beam.

As can be seen in Figure 3.8 with a similar condition, it is possible to increase the angular variation of the mirror: this is due to the fact that, even in the case where a certain variation in pitch or yaw angle causes the collimated beam (is shown in blue in the image) to be positioned at the limit or even outside the lens, a divergent beam (is shown in red in the image) could still pass through the lens and thus reach the sensor.
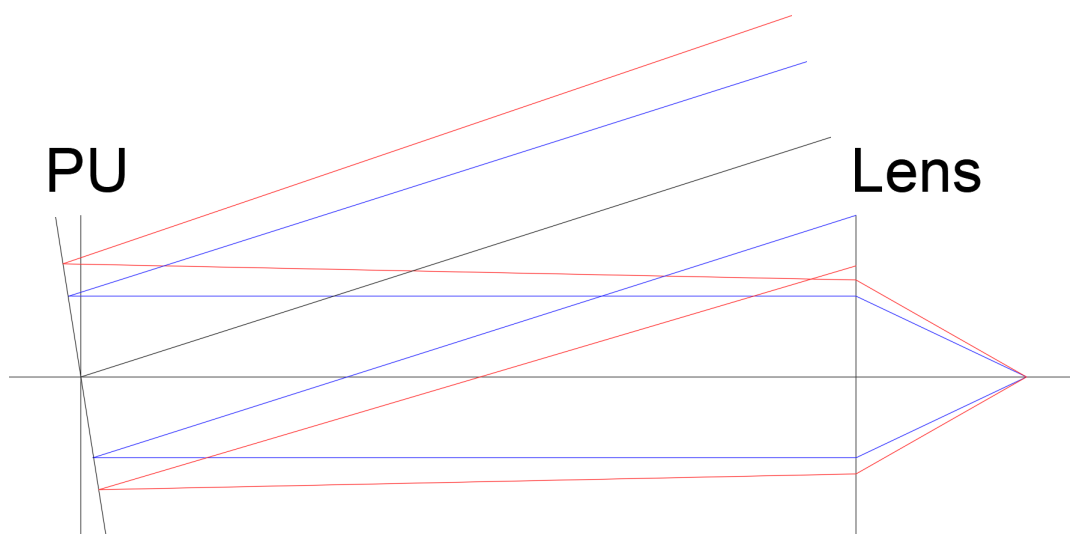
Figure 3.8: Difference between collimating beam and divergent beam

First, the diameter of the collimated beam was measured and found to be 25 mm across the entire path. Next, the first beam splitter was brought closer to the lens so as to obtain a divergent beam diameter at the PU of 50 mm, which covered the entire surface of the last mirror. By means of appropriate geometrical considerations, it is possible to define the half-opening angle of the truncated cone represented by

the laser beam: the latter is approximately 0.09°. This means that, when the laser beam returns to the lens, the latter would have a hypothetical diameter of approximately 75 mm. In reality, however, this cannot be the case because in the current configuration, based on a multiple mirror system, all the light outside the surface of each mirror is lost. For this reason, it was also necessary to increase the laser power in order to achieve intensities comparable to the previous case.

Finally, as the distance between source and lens was shortened, it was necessary to bring the sensor closer to the second beam splitter in order to again obtain as sharp a spot as possible. After doing so, a set of eleven images was acquired with a size of 400x400 pixels with a light spot distance between each image of approximately 30 pixels. As in the previous chapters, the images were 'cleaned' by zeroing the pixels located far from the light spot.

Below is a graph representing the relationship between the horizontal position of the spot and its light intensity:
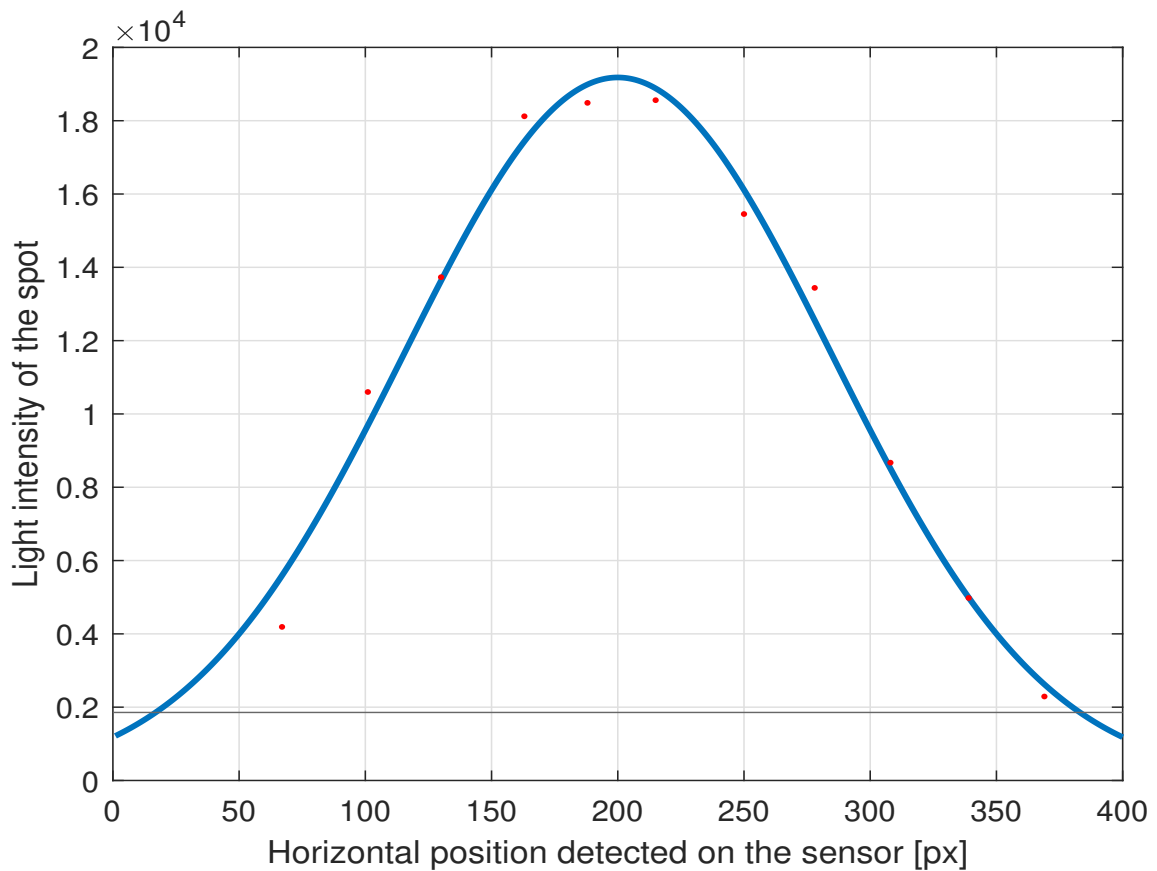
Figure 3.9: Relationship between the horizontal position detected on the sensor and the light intensity in the case of a divergent beam

As can be seen in Figure 3.9, by applying a minimum threshold equal to 10% of the maximum intensity, a horizontal span of approximately 366 pixels was obtained, which, by means of appropriate analytical calculations, corresponds to approximately 0.23291°: this result allows us to confirm that the implementation of a divergent beam allows us to obtain an increase in detectable angles.

3.5 Power reduction with divergent beam

As mentioned earlier, beam divergence causes a reduction in the light intensity of the beam because part of it is outside the lens along the return path. To quantify this reduction, four images were taken, keeping the laser beam orthogonal to the lens and bringing the first beam splitter closer to the lens so as to shorten the distance between the source and the lens, thus obtaining a beam diameter at the PU of 25 mm, 40 mm, 50 mm and 60 mm. In this way it is as if we had obtained return beam diameters at the lens of 25 mm, i.e. the collimated beam condition used as a reference point, 55 mm, 75 mm and 95 mm.

After importing the images into Matlab and 'cleaning' them, the double integrals of the various light spots were calculated in order to define the light intensity detected by the sensor for different beam divergence angles.

Below are the power losses for the different cases analysed expressed in percentage terms:

- Power loss per 40 mm beam diameter on PU: 23.6215%;

- Power loss per 50 mm beam diameter on PU: 33.8616%;

- Power loss per 60 mm beam diameter on PU: 38.5043%.

As expected, if divergence increases, the light intensity detected by the sensor will be lower because the area of the beam that does not impinge on the lens but is outside the lens will be larger. Furthermore, the trend seems to suggest that the reduction in light intensity decreases as the beam diverges.

To try to obtain a useful trend in case one wanted to know how much the power loss might be for beam diameters other than those analysed, the acquired data were interpolated in the Matlab environment. In particular, a zero power loss was considered as long as the laser beam can pass completely inside the lens on the return path net of small positioning errors, thus having a diameter on the PU of approximately 35 mm. Beyond this value, the beam begins to affect the frame of the lens and power losses occur.

The graph representing the interpolation just described is shown below:
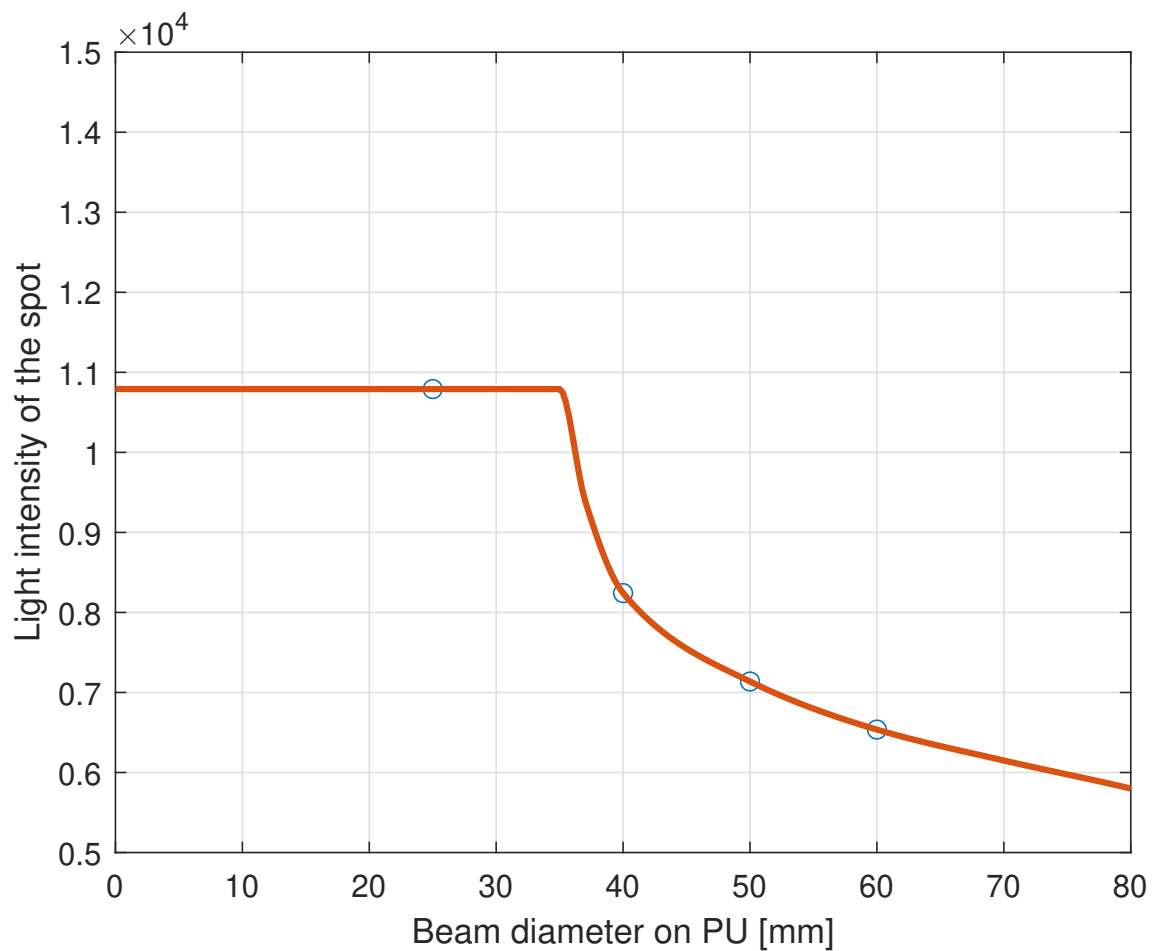
Figure 3.10: Interpolation of acquired power loss data

4. Determination of the roll angle

In the following chapter, the process that led to the practical realisation of a small model, separate from the previous one, for the determination of the roll angle will be explained. The decision to separate this element from the rest of the prototype is due to the desire to make the functioning as clear as possible, thanks to which it is possible to know exclusively the roll angle assumed by the PU without taking into consideration the variations in pitch and yaw angles. It is therefore imagined that this model could subsequently be implemented in the prototype seen above so as to allow the calculation of the three aforementioned angles through a single device.

4.1   Operating principle

The determination of the roll angle is based on the characteristic of electromagnetic waves to exhibit a certain polarisation, i.e. the direction of oscillation of the electric field vector during wave propagation.

The operating principle is illustrated in Figure 4.1. Consider a linearly polarised laser beam passing through a quarter-wave plate which, if orientated correctly, is able to convert the linear polarisation of the beam into circular polarisation. Subsequently, the beam is deflected thanks to the presence of a beamsplitter and reaches the PU where there is a polariser mounted on a mirror which filters the polarisation of the waves in the direction parallel to its axis only: since the polariser rotates together with the mirror, the only oscillation allowed along the return path will

depend on the roll angle assumed by the mirror. When the beam reaches the AU, it again passes through the first beamsplitter and reaches a polarizing beamsplitter cube: this element allows the beam to be separated into two further polarised output laser beams. The beam that is transmitted is characterised by a horizontal polarisation while the reflected beam has a vertical polarisation.

Finally, the two output beams reach two independent photodiodes which, appropriately connected to an oscilloscope, will provide a measurement of the intensity of the incident light for both the transmitted beam and the reflected beam.

With this system, if the PU mirror is oriented at 45° with respect to the polarizing beamsplitter cube, the beam will be divided equally between the two photodiodes which will detect the same intensity: this just described represents the reference configuration, any change in the roll angle of the PU with respect to the reference angle will lead to an unbalanced split of the two polarisations and through the detected difference it will be possible to determine the roll angle of the PU.
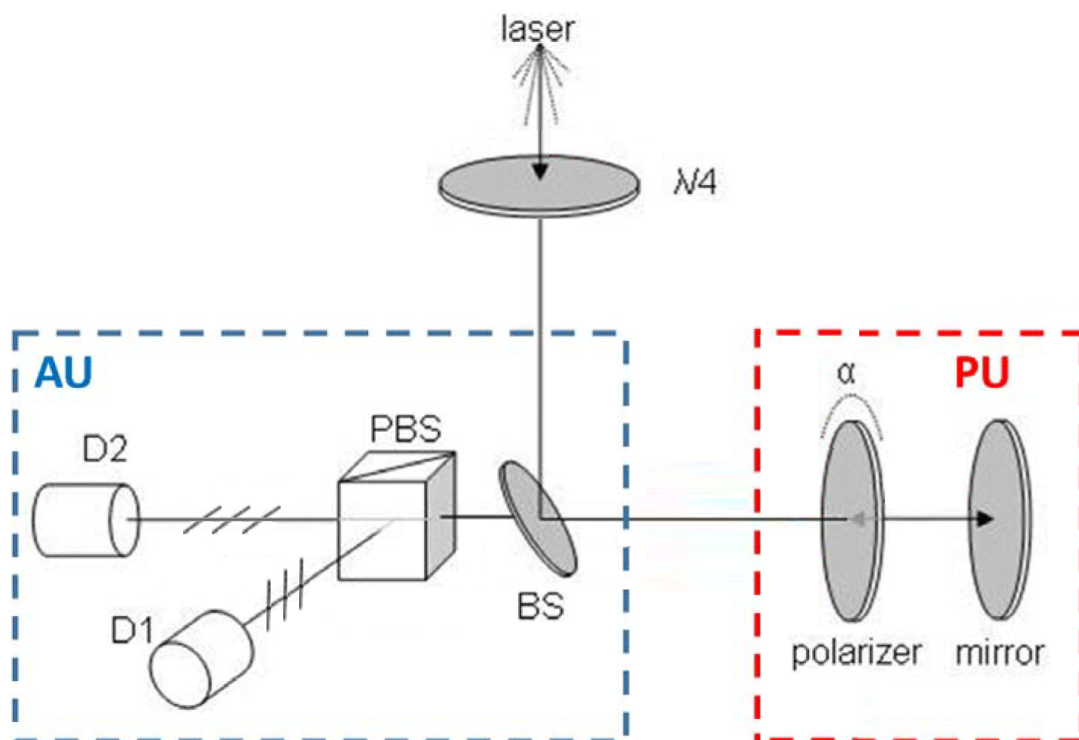
Figure 4.1: Configuration for determining the roll angle in the ATOM project

4.2 Determination of laser polarisation

In order to determine the type of polarisation of the laser beam used, a simplified model of the scheme seen above was created.

The laser used is operating in the red with a wavelength of 633 nm: this choice was determined by the simplicity of using a laser operating in the visible, but the operation is also the same if a laser operating in the infrared is used.

The polariser has been mounted on a motorised stand[9] which allows its automatic rotation by means of a small servomotor. Rotation can take place in single steps or, using a lever, at a constant speed.

After the polariser, a photodiode connected to an oscilloscope was placed, which allows the reading of the detected light intensity expressed in terms of voltage. In addition, to avoid the presence of high-frequency ambient noise, a low-pass filter was also applied, which only allows frequencies below a given threshold to pass through.
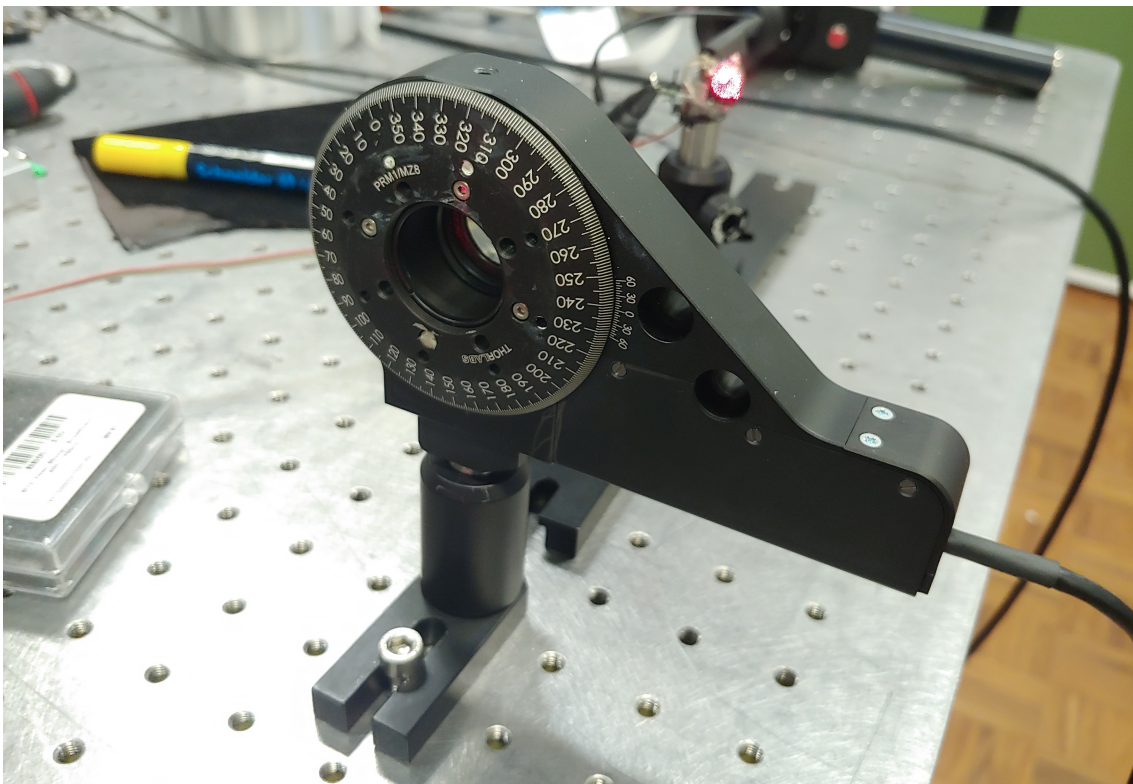
Figure 4.2: Polariser with motorised stand

---

[9]Complete specifications of the motorised stand can be found at [11]
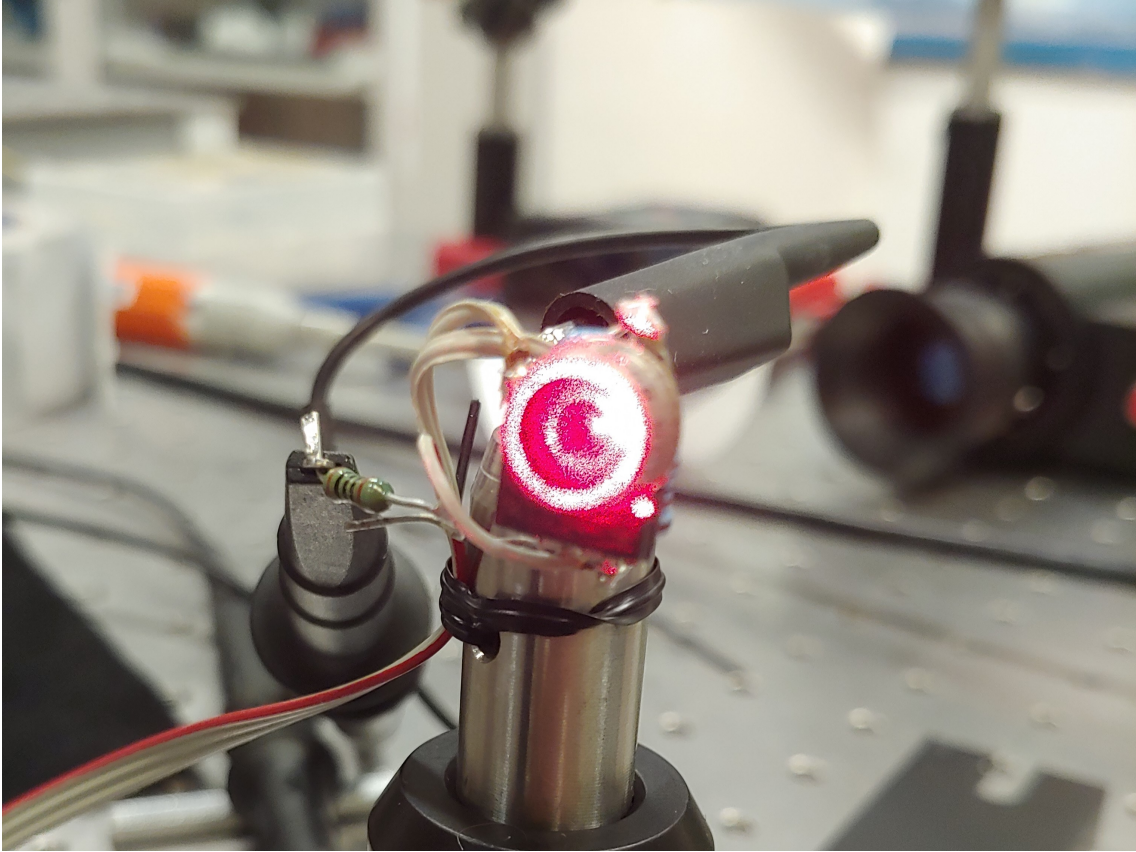
Figure 4.3: Photodiode used for light intensity detection
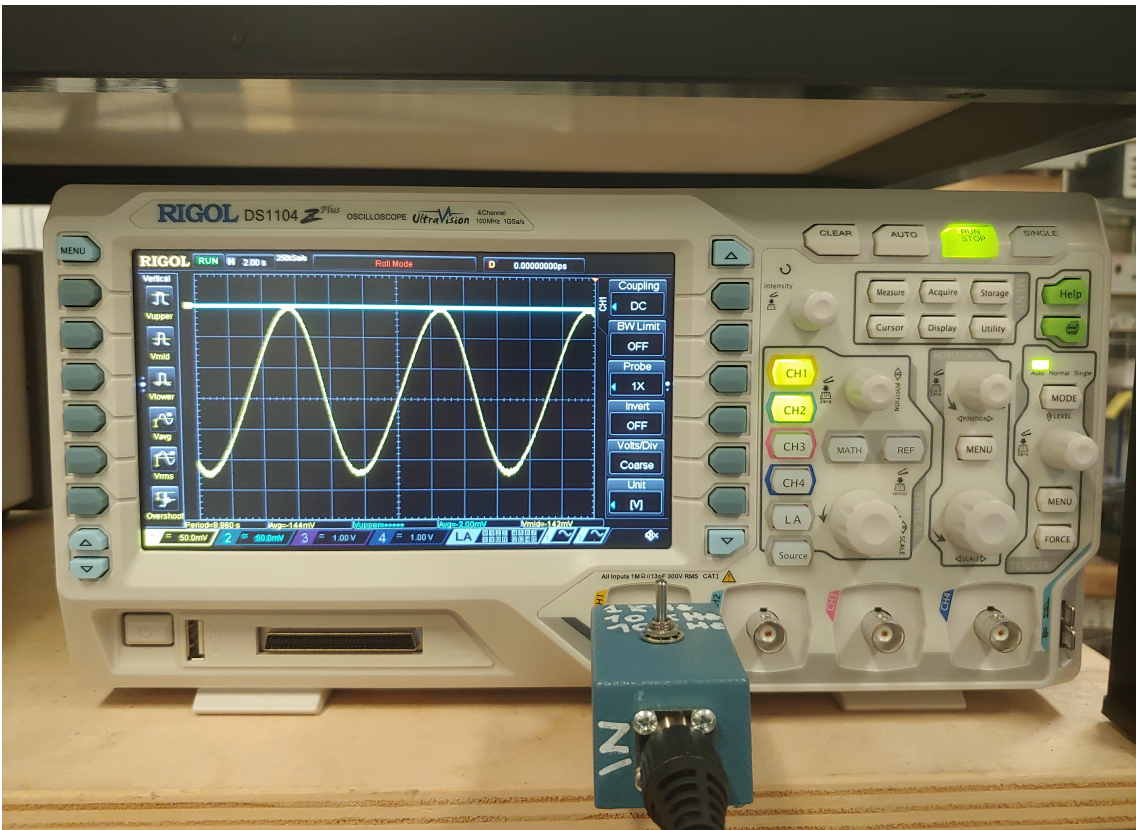
Figure 4.4: Oscilloscope with single photodiode connected and low-pass filter

To verify the type of polarisation characterising the laser used, the latter was only passed through the motorised polariser and the beam was intercepted by a single photodiode connected to the oscilloscope. As can be seen in Figure 4.4, the laser used has a linear polarisation, as the oscilloscope trend is a sinusoidal one, alternating between peaks and null values every 90°: more specifically, the polarisation is vertical, as the peaks are obtained at a null angle of the polariser with respect to the vertical.

4.3 Readings without quarter-wave plate

After determining the type of polarization of the laser used, a polarizing beamsplitter cube produced by ThorLabs[10] was added after the polarizer. Two identical photodiodes with a low-pass filter were placed at the two outgoing beams and connected to the oscilloscope.
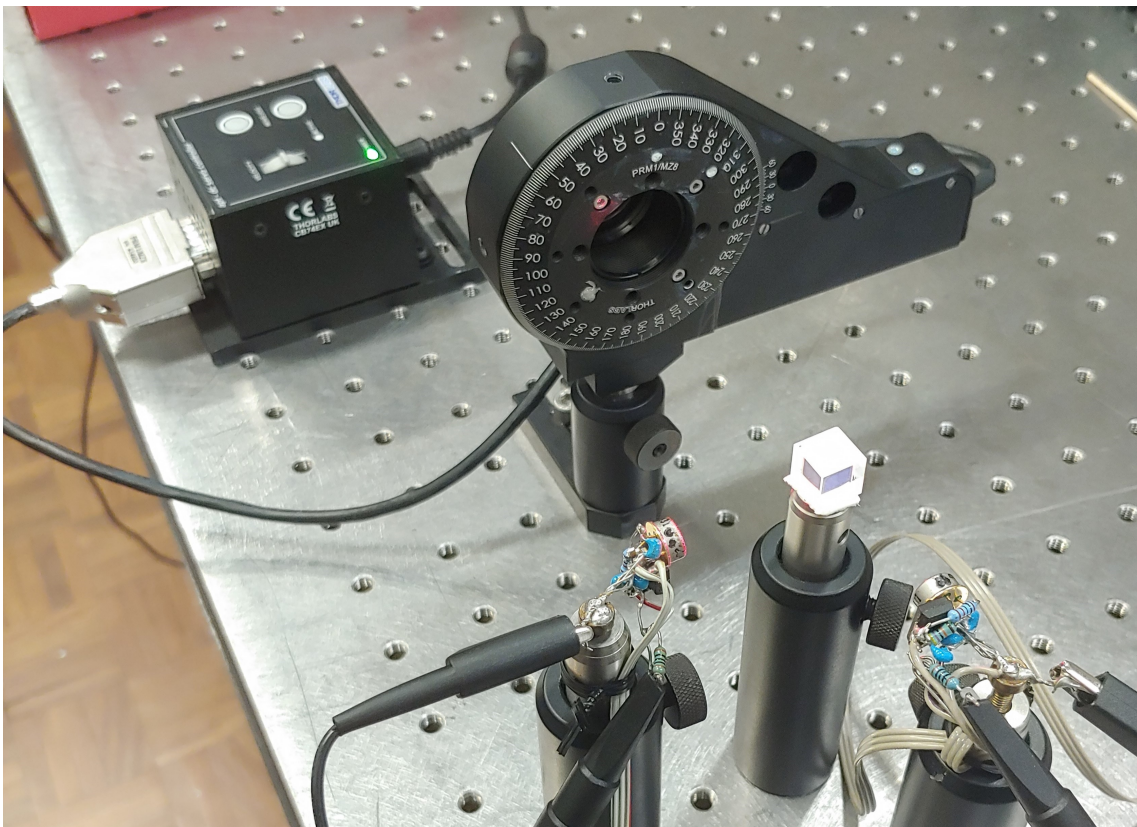
Figure 4.5: Practical model for determining the roll angle without the quarter-wave plate

---

[10]Complete specifications of the polarizing beamsplitter cube can be found at [10]
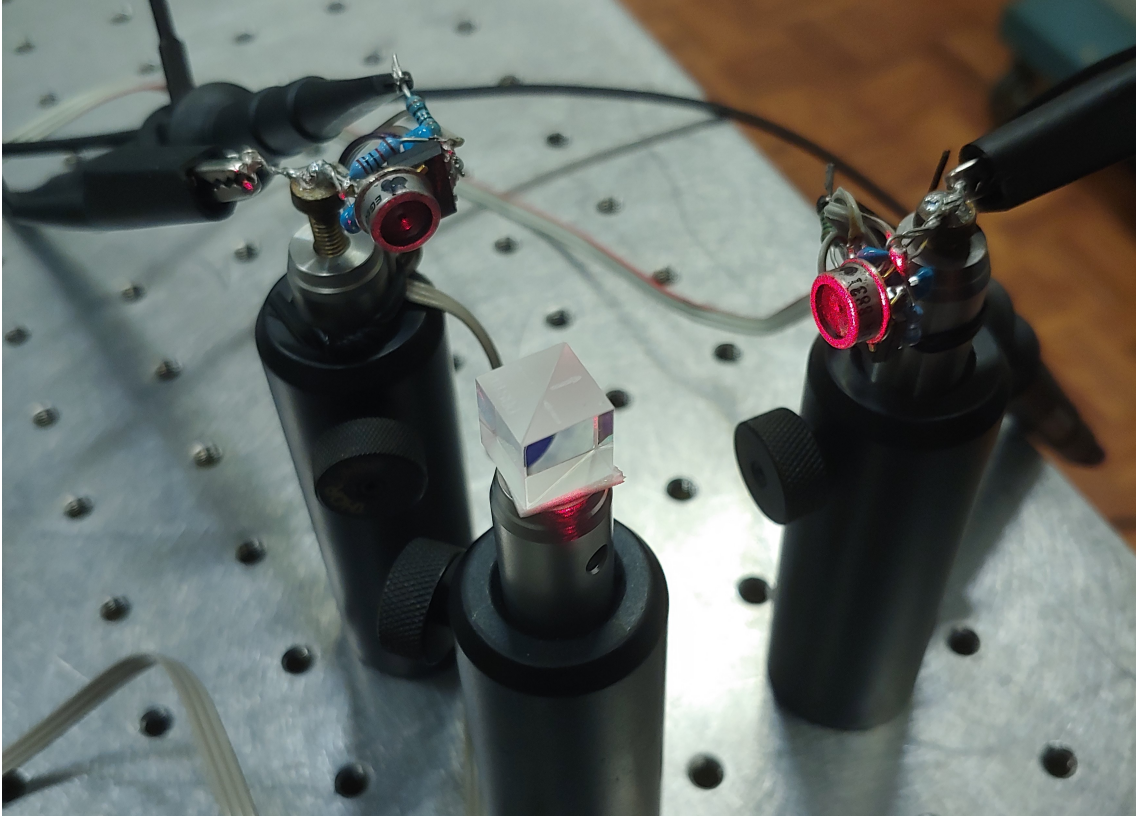
Figure 4.6: Polarizing beamsplitter cube with two photodiodes at the outgoing beams
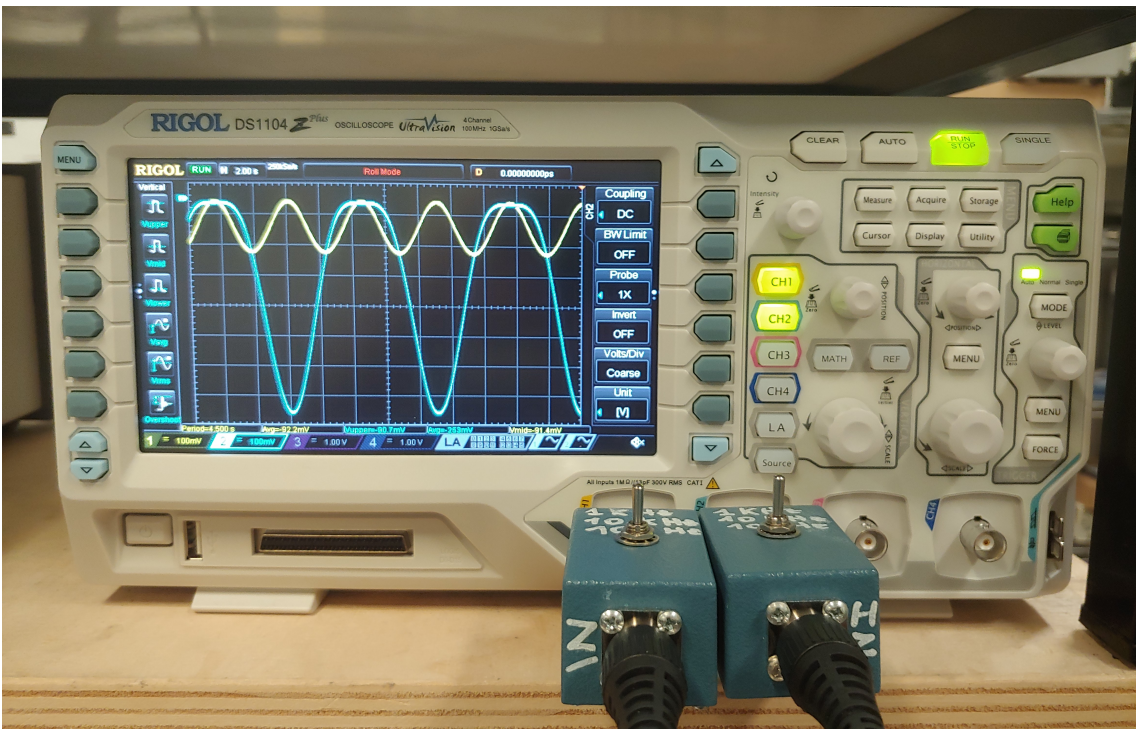
Figure 4.7: Oscilloscope readings with two connected photodiodes and low-pass filters without quarter-wave plate

Subsequently, the data taken from the oscilloscope was taken and imported into the Matlab environment. In this way, it was possible to obtain a graph relating the angle assumed by the polariser to the intensities coming out of the polarizing beamsplitter cube.
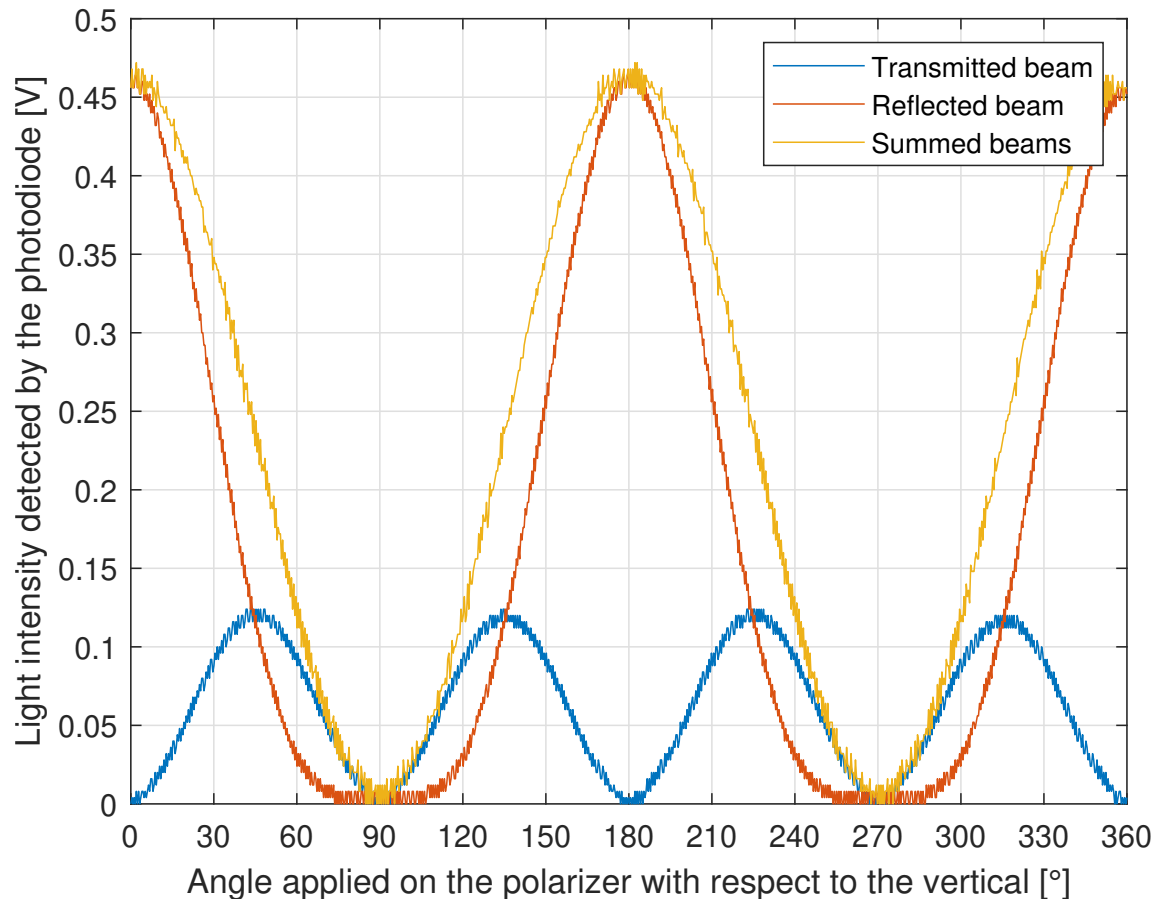
Figure 4.8: Relationship between the angle assumed by the polariser and the intensities exiting the polarizing beamsplitter cube without quarter-wave plate

As mentioned above, the beam transmitted by the polarizing beamsplitter cube corresponds to the horizontal polarisation while the reflected beam corresponds to the vertical polarisation: this can also be deduced by looking at Figure 4.8 alone, since when the polariser is at 0° the polarisation detected must be only the vertical one.

The trend detected by the two photodiodes is justified by Malus's law[7] which states that the luminous intensity of a light ray passing through a polarising filter, whose axis of polarisation forms an angle θ with the plane of vibration of the light wave, is given by the relation $I = I_0 cos^2\theta$ where I_0 is the incoming intensity and I is

the intensity exiting the filter which will have an angle equal to that of the polariser.
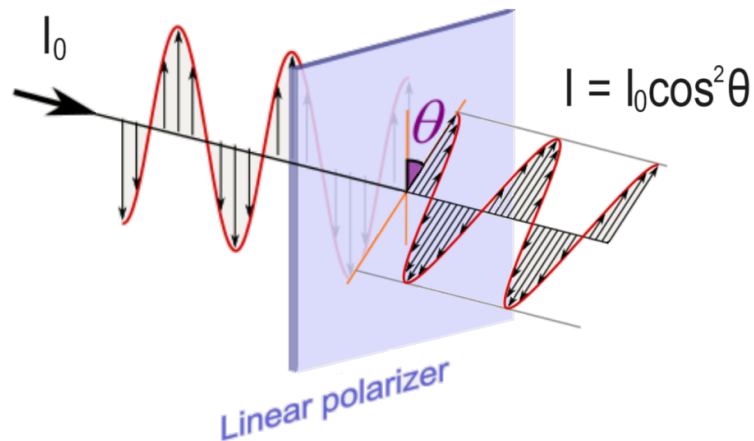
Figure 4.9: Principle of operation of a linear polariser - Malus Law

It follows then that if we consider a rotation of the polariser from 0° to 90° with a step of 10°, we obtain a pattern as depicted in Figure 4.10:

- when the polariser has an orientation equal to 0° with respect to the polarisation of the laser, the output beam presents only vertical polarisation (represented in red), consequently the horizontal polarisation (represented in green) is zero;

- subsequently, as the polariser rotates, the overall light intensity decreases (rapresented in black) and, more specifically, the intensity of the beam with vertical polarisation continues to decrease as polariser rotates while the intensity of the beam with horizontal polarisation increases up to 45° after which it also decreases;

- when the polariser is at 90° with respect to the polarisation of the laser the overall light intensity is zero.

As can be seen, this behaviour is the same as that in Figure 4.8 and summing up the two signals results in a sinusoidal pattern that corresponds exactly to that seen previously in the case where the polarizing beamsplitter cube was not present.
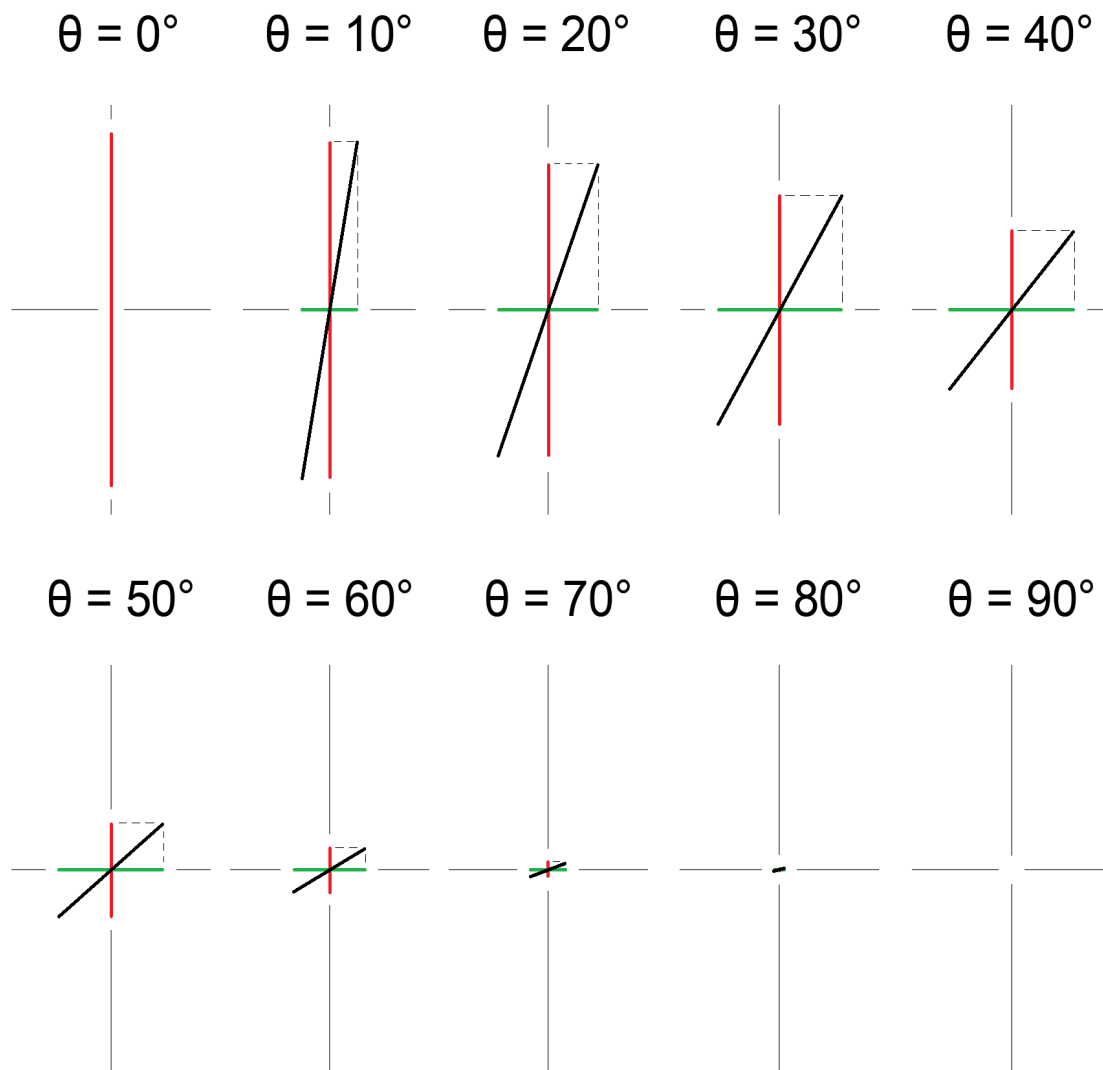
Figure 4.10: Variation in luminous intensity for every 90° change in polariser orientation

4.4   Introduction of quarter-wave plate

Subsequently, the quarter-wave plate[11] was also introduced in order to achieve circular polarisation. The plate used is specific to the chosen wavelength and was mounted on a holder that allows its orientation to be varied. This is necessary because linear polarisation is only transformed into circular polarisation if the axis of the quarter-wave plate has an angle to the laser polarisation of 45°. If this condition is not met, an elliptical polarisation would be obtained instead of a circular one.

[11]Complete specifications of the quarter-wave plate can be found at [12]

Figure 4.11: Quarter-wave plate
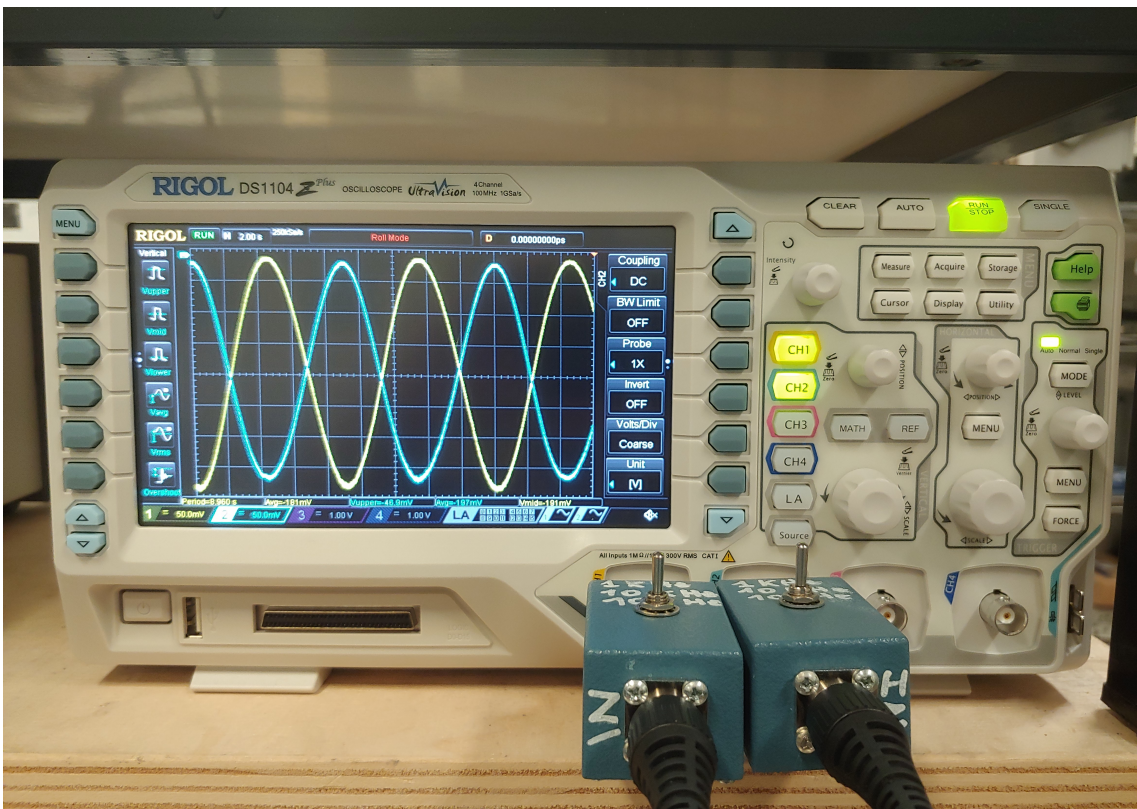
Figure 4.12: Oscilloscope readings with two connected photodiodes and low-pass filters with quarter-wave plate

The data acquired from the oscilloscope was imported into the Matlab environment and, as done previously, a graph was created relating the angle assumed by the polariser to the intensities exiting the polarizing beamsplitter cube considering also the quarter-wave plate.
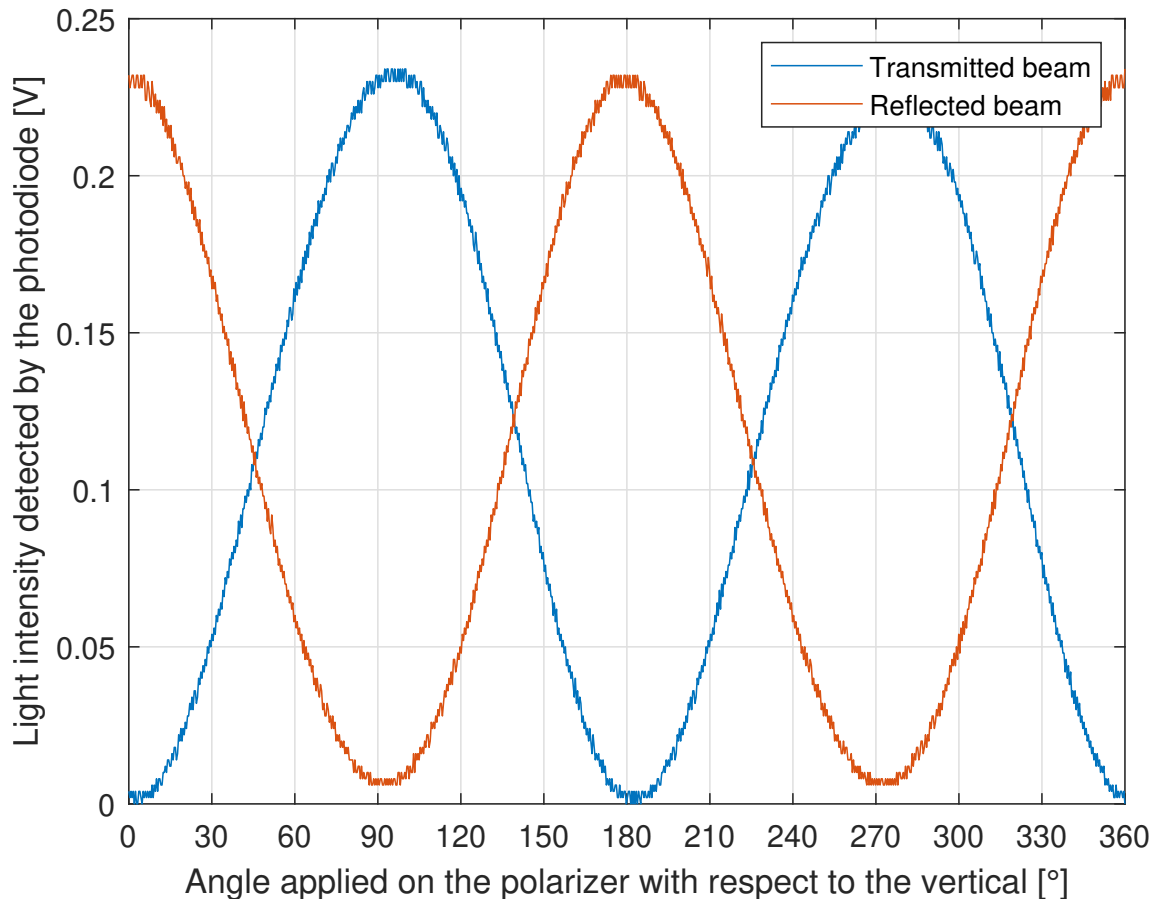
Figure 4.13: Relationship between the angle assumed by the polariser and the intensities exiting the polarizing beamsplitter cube with quarter-wave plate

As can be seen in Figure 4.13 the transmitted beam and the reflected beam both present a sinusoidal trend with the same amplitude: this is due to the fact that, having obtained a circular polarisation, the intensity at the output of the polariser does not decrease as the angle applied to it varies. This results in an alternation between maximum peaks and null values, obtaining two identical trends offset by 90°. In this way, every 45° the two outgoing beams will present the same intensity and this condition will be used as a reference point: if the PU varies its roll angle, the two beams coming out of the polarizing beamsplitter cube will no longer present the same intensity and, knowing how much the difference in intensity between the

two beams is, it will be possible to obtain the roll angle assumed by the PU.

To do this, the two curves representing the intensity of the transmitted and reflected beam were interpolated to derive two sinusoidal functions and then the difference between these two was calculated: as can be seen in Figure 4.14, the difference between the two functions is also a sinusoidal function.
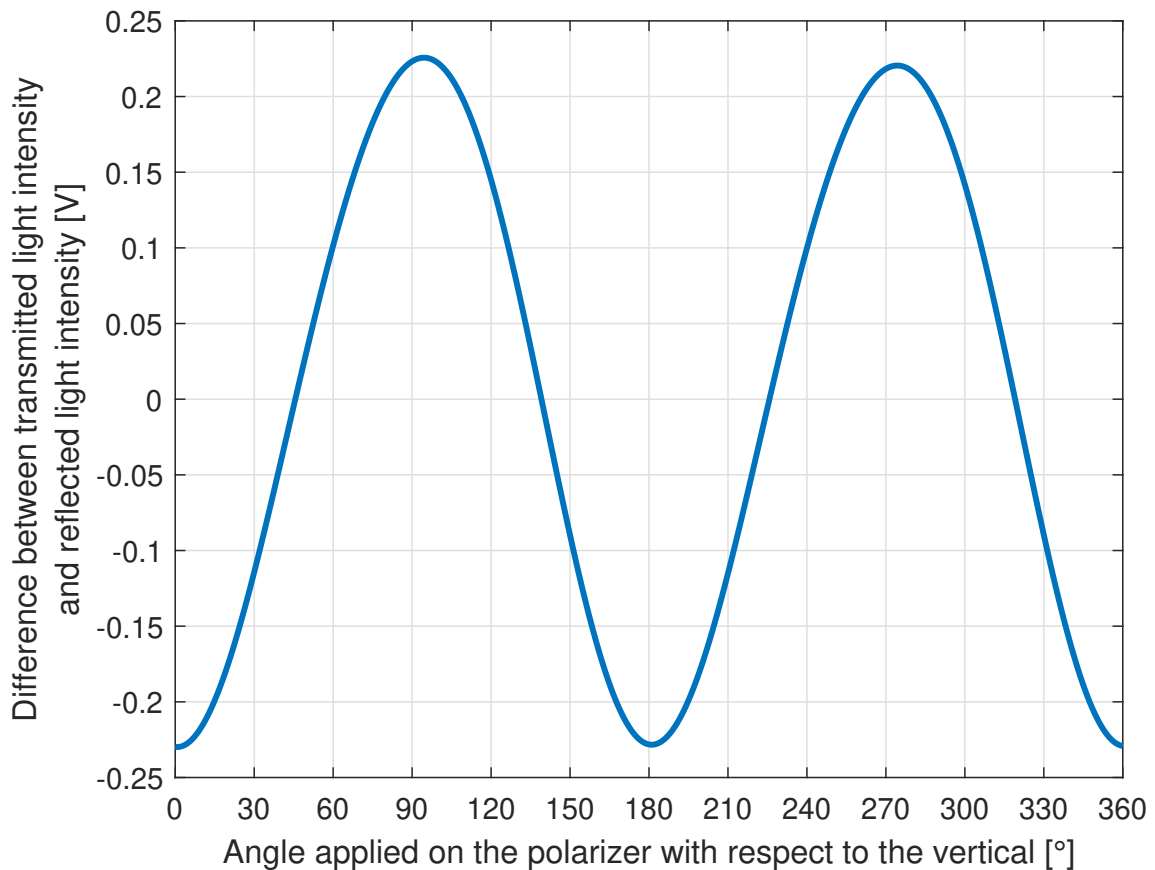
Figure 4.14: Relationship between the angle assumed by the polariser and the difference between transmitted intensity and reflected intensity

By focusing on the area where this function is zero, it is possible to determine how much the change in the PU's roll angle is based on the values on the y-axis: for example, looking at Figure 4.15 it is possible to state that if the voltage difference between the transmitted and reflected intensity is 0.003 V then the PU is in a condition where its roll angle is 46° from the vertical.

For the sake of completeness, the graph representing the normalised difference is also shown in Figure 4.16.
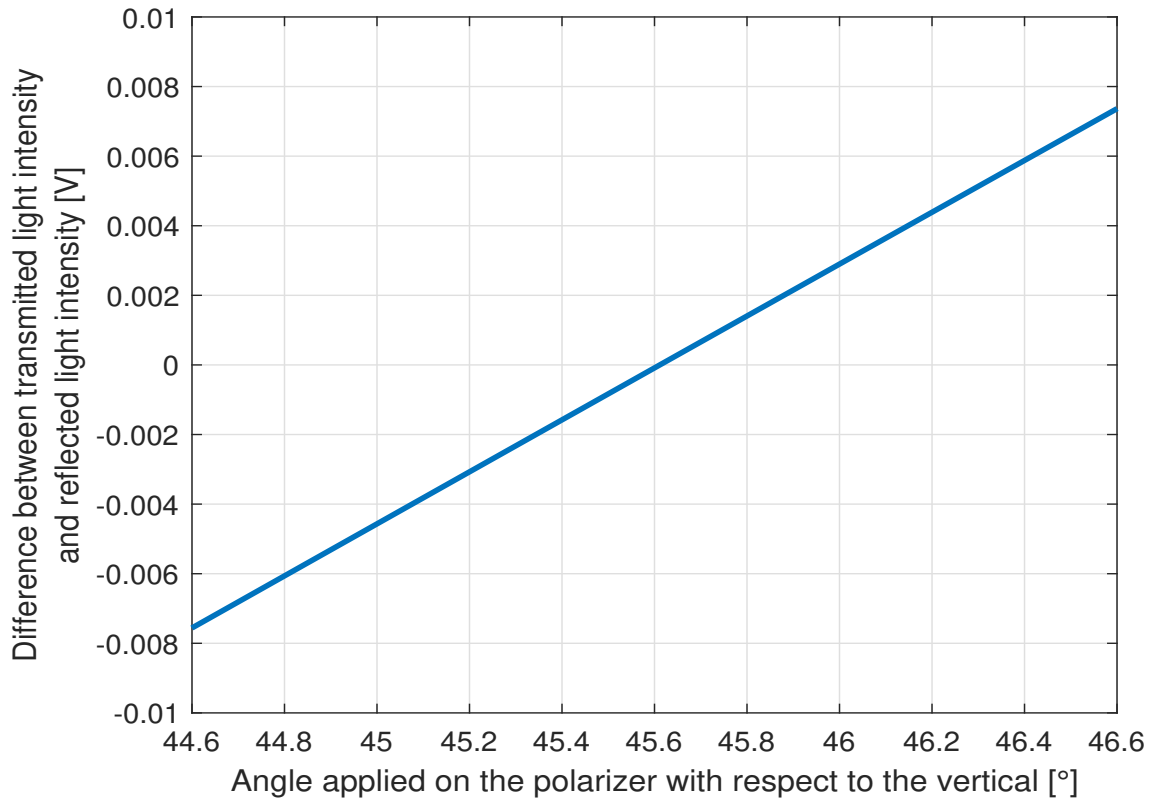
Figure 4.15: Difference between transmitted intensity and reflected intensity - Reference point
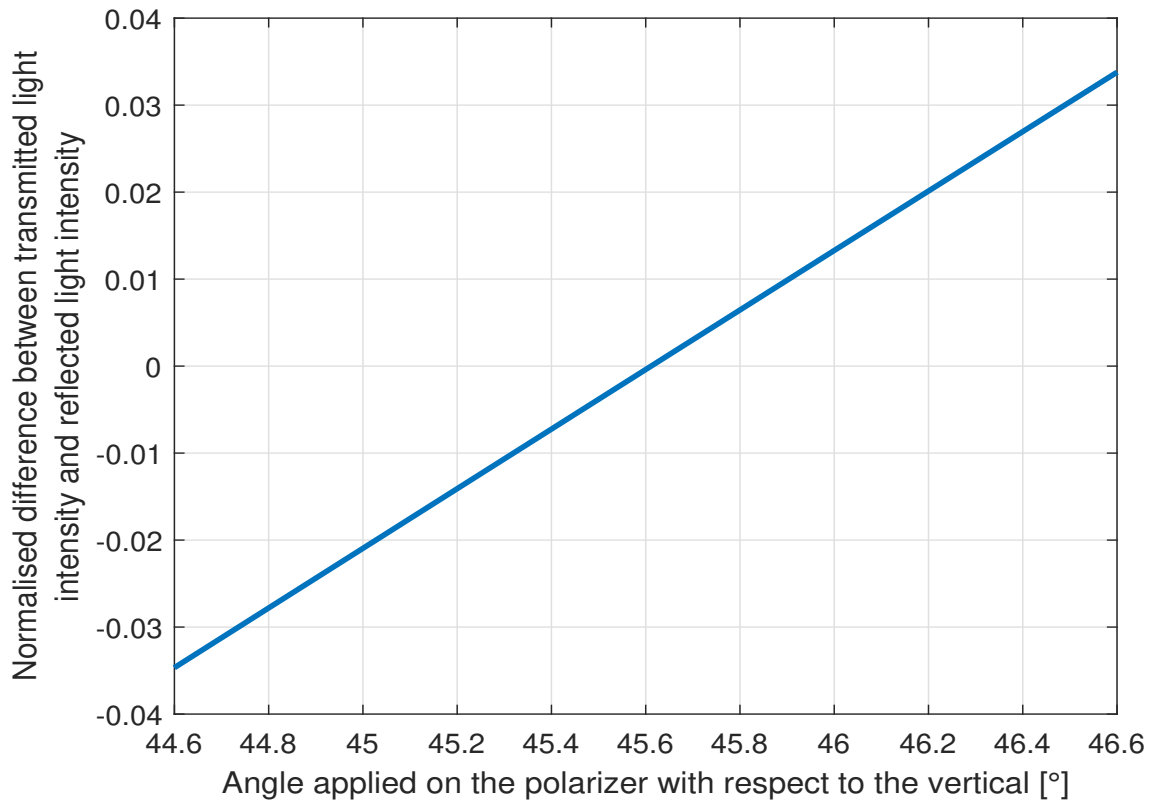
Figure 4.16: Normalised difference between transmitted intensity and reflected intensity - Reference point

5. Conclusions

In the present thesis work, a prototype of the INRiM-designed sensor based on optical metrology was realised to cope with the growing trend in the use of large reflectors in telecommunication satellites. Given the innovative method, this study focused on verifying the requirements of the ATOM project. The objectives achieved are described below:

- with the configuration proposed by INRiM, under collimated beam conditions using a lens with a diameter of 50 mm and placing the target approximately 8 m from it, it was possible to detect a variation in the yaw and pitch angles of the target of approximately $\pm 0.09°$. This result can be considered satisfactory despite being slightly inferior to ESA's expectations, which required a yaw and pitch angle variation of at least $\pm 0.1°$;

- In order to achieve the objective imposed by ESA, the configuration was slightly modified so as to no longer obtain a collimated beam but a divergent beam. In this way, with the same number of elements used, it was possible to increase the conditions such that the beam returned to the lens and was detected by the sensor, obtaining a detection of yaw and pitch angles equal to approximately $\pm 0.116°$. This result allows us to state that it is possible to meet the requirement imposed by ESA and exceed it by a good margin;

- with regard to the roll angle, ESA required the possibility of being able to detect a variation of several degrees. As seen above, the method for detecting

the roll angle in no way limits the conditions under which this is possible and, hypothetically, any type of variation can be detected, both clockwise and counter-clockwise.

In addition, the following remarks are made:

- the measurements of yaw and pitch angles and roll angle were carried out using two different models, and a future study could involve the implementation of a single compact model through which all three angles could be measured;

- as mentioned above, a laser operating in the red was used for the detection of the roll angle, whereas the project envisages the use of infrared lasers: although the operating principle is the same and leads to the same results, the implementation described in the previous point, which would make use of infrared only, would allow these results to be confirmed even under design conditions;

- finally, the development of a compact frame suitable for the spatial environment capable of containing all the elements used is envisaged. A possible expansion of this work could consist in re-performing the measurements and confirming the results obtained directly using the sensor which will then be mounted on the satellites or an embryonic phase of the latter.

References

[1] *19.5AC-0-FC Bulkhead fiber adapter FC PC to system mount Ø 19.5 mm with TILT alignment*. URL: https://www.sukhamburg.com/products/details/19_5AC-0-FC.

[2] *AL50100H - Ø50.0 mm Diffraction-Limited N-BK7 Aspheric Lens, f = 100.0 mm, NA = 0.20, Uncoated*. URL: https://www.thorlabs.com/thorproduct.cfm?partnumber=AL50100H.

[3] *EBS2 - Economy 50:50 Beamsplitter, Ø2", AOI: 45°*. URL: https://www.thorlabs.com/thorproduct.cfm?partnumber=EBS2.

[4] *ELCOMAT 5000 - Electronica autocollimator*. URL: https://moeller-wedel-optical.com/en/product/elcomat-5000/.

[5] *KM100 - Kinematic Mirror Mount for Ø1" Optics*. URL: https://www.thorlabs.com/thorproduct.cfm?partnumber=KM100#ad-image-0.

[6] *KM200 - Kinematic Mirror Mount for Ø2" Optics*. URL: https://www.thorlabs.com/thorproduct.cfm?partnumber=KM200#ad-image-0.

[7] *Malus's law and other properties*. URL: https://en.wikipedia.org/wiki/Polarizer#Malus'_law_and_other_properties.

[8] *Onsemi 1/2.5-Inch 5 Mp CMOS Digital Image Sensor MT9P031*. URL: https://www.onsemi.com/pdf/datasheet/mt9p031-d.pdf.

[9]   *P1-630PM-FC-2 - PM Patch Cable, PANDA, 630 nm, FC/PC, 2 m*. URL: https://www.thorlabs.com/thorproduct.cfm?partnumber=P1-630PM-FC-2.

[10]   *PBS102 - 10 mm Polarizing Beamsplitter Cube, 620 - 1000 nm*. URL: https://www.thorlabs.com/thorproduct.cfm?partnumber=PBS102.

[11]   *PRM1/MZ8 - Ø1" Motorized Precision Rotation Stage (Metric)*. URL: https://www.thorlabs.com/thorproduct.cfm?partnumber=PRM1/MZ8#ad-image-0.

[12]   *WPQ05ME-633 - Ø1/2" Mounted Polymer Zero-Order Quarter-Wave Plate, SM05-Threaded Mount, 633 nm*. URL: https://www.thorlabs.com/thorproduct.cfm?partnumber=WPQ05ME-633.